Quantum state transfer between valley and photon qubits

Ming-Jay Yang,[1] Han-Ying Peng,[2] Neil Na,[3] and Yu-Shu Wu[1,2]
[1]*Institute of Electronics Engineering, National Tsing-Hua University, Hsinchu 30013, Taiwan*
[2]*Department of Physics, National Tsing-Hua University, Hsinchu 30013, Taiwan*
[3]*Artilux Inc., Zhubei City, Hsinchu 30288, Taiwan*
(Received 7 October 2016; revised manuscript received 30 December 2016; published 7 February 2017)

The electron-photon interaction in two-dimensional materials obeys the rule of "electron valley–photon polarization" correspondence. At the quantum level, such correspondence can be utilized to entangle valleys and polarizations and attain the transfer of quantum states (or information) between valley and photon qubits. Our paper presents a theoretical study of the interaction between the two types of qubits and the resultant quantum state transfer. A generic setup is introduced, which involves optical cavities enhancing the electron-photon interaction as well as facilitating both the entanglement and unentanglement between valleys and polarizations required by the transfer. The quantum system considered consists of electrons, optically excited trions, and cavity photons, with photons moving in and out of the system. A wave equation based analysis is performed, and analytical expressions are derived for the two important figures of merits that characterize the transfer, namely, yield and fidelity, allowing for the investigation of their dependences on various qubit and cavity parameters. A numerical study of the yield and fidelity has also been carried out. Overall, this paper shows promising characteristics in the valley-photon state transfer, with the conclusion that the valley-polarization correspondence can be exploited to achieve the transfer with good yield and high fidelity.

DOI: 10.1103/PhysRevB.95.075407

I. INTRODUCTION

The valley degree of freedom in electrons has recently attracted a lot of attention, in particular in two-dimensional (2D) hexagonal materials such as graphene [1–3] and transition metal dichalcogenides (TMDCs) [4–7]. In addition to its unique electromagnetic properties [1–3], this degree of freedom also manifests novel optical behaviors [4–8]. Altogether, a wide spectrum of exciting opportunities is created for the valley-based electronics known as valleytronics.

In the class of 2D hexagonal materials [9–12], the threefold rotational symmetry comprises the physical root of the intriguing valley-dependent physics. Basically, in the presence of an energy gap, the constraint of symmetry on electron states results in intrinsic, unit-cell-scale orbital angular momenta with opposite signs for electrons in the Dirac valley doublet at K and K′ of the Brillouin zone [2,8]. In close analogy to the ordinary electron spin, where opposite angular momenta characterize up and down states, a valley pseudospin thus emerges with index given by, for example, $\tau_v = +1$ for K and -1 for K′, which fully qualifies for the role of a quantum bit carrier as the electron spin does. In particular, concrete proposals have been given of a valley-based approach to the fundamental unit, namely, a qubit, for the application of quantum information processing [13–17] based on quantum dots (QDs) [18–20]. In the case of graphene, for example, the valley degree of freedom can be incorporated to expand an electron spin qubit to a spin-valley qubit [14], or one can freeze out the spin and construct a valley-pair qubit out of a pair of QDs, with each QD localizing an electron and subject to the modulation of both an external magnetic field and electrical gates for qubit manipulation [13]. Demonstration has been given in the latter case, showing the satisfaction of DiVincenzo criteria for universal quantum computing.

In a way similar to semiconductor electron spin qubits [21], valley qubits can interact with photon qubits with a good coupling strength. Such an interqubit interaction is characterized by several promising features. First, the 2D materials of interest have direct band gaps at Dirac points allowing for strong, vertical optical transitions. In the case of graphene, a large optical matrix element $\sim e v_F A$ exists for the transition, due to the sizable v_F (v_F = Fermivelocity $\sim 10^6$ m/sec, e = electroncharge, A = vectorpotential). In addition, valley qubits can be integrated with cavities or waveguides of planar photonic structures [22,23] for an enhancement of the electron-photon (e-ph) interaction. In fact, control of the interaction in 2D materials using cavities has been demonstrated under both strong [24] and weak [25] coupling regimes, which paves the path for implementing photon-valley interfaces required for valley-involved optoelectronics.

The valley-photon interaction physics is significantly enriched by the existence of a valley-dependent selection rule for optical transitions. Due to the presence of finite valley and photon angular momenta, the law of angular momentum conservation leads to interband transitions that are governed by the valley-dependent selection rule, as shown in Fig. 1 with the involved photons being circularly polarized. Because of this selection rule, an approximate one-to-one correspondence exists between circular polarizations of pumping (emitted) photons and valley states of excited (recombining) electron-hole pairs [4–8]. Experimentally, the past few years have seen great strides in the field of optovalleytronics in spin-valley pumping by optical excitations that utilize the selection rule [4–7]. From the perspective of quantum information processing, the valley-polarization correspondence is also of great interest. Since this correspondence implies the existence of a natural quantum state transfer (QST) between photon and valley qubits [26], a theoretical and experimental raise of its utilization via such QST to the quantum information processing level of applications would fulfill the full potential of the correspondence.

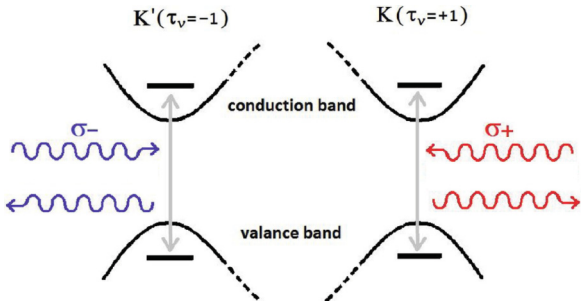

FIG. 1. Approximate selection rule for the interband optical transition in gapped graphene. $\sigma_{+(-)} = \sigma_x + (-)i\sigma_y$ denotes circular polarization states in the graphene plane.

The QST is a coherent quantum process where, via the e-ph interaction, the photon state information can be extracted and stored in a valley qubit, and the reverse process that moves the state information of a valley qubit back to a photon can as well occur. Such valley-photon QST provides an analogy to the well-studied spin-photon QST [27]. In the latter case, for example, a coherent single photon detection is realized via the process of photon absorption, electron-hole pair generation, and hole extraction, leaving the polarization state of the photon totally encoded in the spin of the excited electron. On the other hand, the valley-photon QST also constitutes an interesting contrast to the spin-photon QST, with the following fundamental difference existing between the two.

In the electron spin case, a single spin forms the simplest qubit in the class of spin qubits and hence has been the focus of spin-photon QST studies; whereas, in the valley case, a pseudospin qubit must consist of two valley pseudospins with the states being given by the so-called decoherence-free singlet/triplet states [28]. Therefore, this valley-pair qubit makes a natural choice for valley-photon QST, and the corresponding study would, from the scientific perspective, constitute an attempt at understanding the nature of QST between photons and the class of decoherence-free qubits.

From the application point of view, the study of valley-photon QST would also advance the field of quantum technology in 2D materials. For example, this specific QST would facilitate the development of valley-involved quantum tomography, where one can reconstruct the valley (photon) state via a measurement done on the photon (valley) state, when the latter is easier to characterize than the former. In addition, it is well suited to the application of quantum communications (QCs) [26], with a potential to realize the quantum repeater (QR) protocol as follows. A QR extends the distance of QCs beyond that of photon attenuation by an iterative process involving the QST from photons to quantum memories (static forms of qubits) and eventually sets up a global entanglement required for quantum teleportation [29,30]. For such an application, the QST involved is required to be as faithful as possible since any state distortion during the transfer would lead to a corresponding reduction in the degree of entanglement and hence loss of fidelity in the information teleported. From such a perspective, quantum memories can be implemented with only a few physical systems. For instance, coherent state transfer and control in atomic and ionic systems has made a great progress [31–34]; superconducting qubits with transmission line cavities in circuit quantum electrodynamic setup offer the possibility of large-scale, fault-tolerant quantum information processing with integrated qubits [35]; the electronic spin triplet ground state in a nitrogen-vacancy defect exhibits a promising long decoherence time [36,37]; for QD-confined electron spin qubits, the state transfer from photon polarization to electron spin using optically active semiconductor QDs has been extensively studied and demonstrated [38,39]. Like these systems, valley qubits also carry properties that qualify them for quantum memories. For valley qubits, one represents logical 0 and 1 with the low energy sector of states where the dynamical variables consist only of valley pseudospins of electrons. Such qubits have the advantage that the large wave vector difference between K and K′ valleys stabilizes the qubit state and provides a good coherence protection, with valley relaxation time for such qubits to be in the range of $10^{-6} \sim 10^{-3}$ sec under reasonable conditions [13,26]. However, it should be noted that the simplest realization of a valley qubit with a single valley pseudospin may be quite challenging. With the qubit state space $\{0, 1\}$ represented by the two-state space $\{K,K'\}$ of the pseudospin, such a qubit faces the issue of being difficult to transform between, for example, K and K′ via controllable means due to the wave vector difference between them. This difficulty would have to be overcome in applications involving qubit state manipulations, as in the case of QRs when setting up the global entanglement [29,30]. On the other hand, a valley-pair qubit with two valley pseudospins resolves such an issue [13]. In this case, spin and orbital degrees of freedom are removed by a magnetic field-induced spin quantization and the QD confinement-induced localization, respectively. The remaining degrees of freedom, i.e., the two localized pseudospins, interact with each other via a spin exchange type coupling and form the two maximally entangled states, namely, the valley singlet state $|Z_S\rangle = \frac{1}{\sqrt{2}}(|K_L K'_R\rangle - |K'_L K_R\rangle)$ (with subscripts L and R denoting the left and right QDs, respectively) and the valley triplet state $|Z_{T_0}\rangle = \frac{1}{\sqrt{2}}(|K_L K'_R\rangle + |K'_L K_R\rangle)$. The two states can represent 0 and 1, respectively, and a single-qubit transformation in the $\{0,1\}$ space can be performed without any valley flipping [13], as described in the following in terms of the Bloch sphere representation of qubit states. First, the exchange coupling between the QDs can be electrically controlled to rotate the qubit around one axis of the sphere. Second, a mechanism called valley-orbit interaction (VOI) exists between the valley pseudospin and an in-plane electric field. This field can be induced by electrical gates near the QDs to allow, via the VOI mechanism, for rotation of the qubit around another axis of the sphere. The two foregoing independent rotations can be combined to achieve an arbitrary single qubit manipulation on the time scale of 10^{-9} sec under reasonable conditions [13,26]. Such an electrical gated valley qubit features scalability similar to typical solid state qubits and can be advantageous to the implementation of quantum error correction (QEC) coding [40,41]. Due to the fact that the QEC represents a single logical qubit with a cluster of physical qubits, construction of the corresponding circuit can be facilitated by the scalability of valley qubits.

The photon-valley QST is a complicated quantum-mechanical problem. It involves a system of valley qubit electrons, optically excited electrons and holes, and

photons, with the e-ph coupling existing between the particles. Moreover, the system is open and communicates with the external world via the photonic signal moving in and out of the system. The present paper provides an initial, yet semiquantitative, understanding of this complicated problem through an analytical approach based on a set of approximations. It introduces a generic setup for the photon-valley QST that can be optimized for the yield and fidelity and investigates the QST in a sophisticated quantum-mechanical model beyond what is merely based on the approximate valley-polarization correspondence. Specifically, the setup consists of the valley qubit being placed inside both a distributed Bragg reflector (DBR) based cavity and a photonic crystal (PC) cavity. The DBR cavity serves to enhance the e-ph interaction for the absorption of incoming signal photon by the valley qubit and so facilitates the valley-polarization entanglement. The PC cavity serves to enhance the photon emission from the photo-excited valley qubit as well as project the linear polarization state of the emitted photon and so facilitates the valley-polarization unentanglement. Through the entanglement and unentanglement processes, the quantum state information of the incoming photon is shared with and transferred to the valley qubit. A quantum-mechanical analysis is performed for such processes in terms of realistic optical matrix elements and a reasonable phenomenological modeling of damping for both the electron states and cavity modes, yielding quantum-mechanical equations that govern the time evolution of various probability amplitudes in the system. These amplitudes are analytically solved to determine the expressions of yield and fidelity: The fidelity measures the fraction of faithful QST per transfer, and the yield describes the fraction of photon-to-quantum memory conversion per incoming signal photon. These two figures are the upmost important parameters that determine the efficiency and resources involved in the QST. Their explicit dependences on various cavity and qubit parameters are derived to facilitate our investigation of the optimal conditions for yield and fidelity. A numerical study of the yield and fidelity is also carried out. Overall, the study shows promising characteristics in the photon-valley QST, with the conclusion that the valley-polarization correspondence can indeed be exploited to achieve such a QST with good yield and high fidelity.

The paper is organized as follows. In Sec. II, we first describe the setup designed to both enhance the e-ph interaction and differentiate the incoming and outgoing photons. We then discuss the optical matrix element and provide a description of the photon-valley QST in the setup. In Sec. III, we present a quantum-mechanical description of the QST process, solve the quantum-mechanical equations, and derive the analytical expressions of yield and fidelity. In Sec. IV, based on the expressions of yield and fidelity, numerical results are obtained, and their implications are discussed for the photon-valley QST in the proposed setup. In Sec. V, we summarize our findings. In the Appendix, we provide the mathematical details involved in solving the various probability amplitudes.

II. PHOTON-VALLEY QST IN CAVITIES

Section II A overviews the QST in a simple setup with a single optical cavity. Section II B discusses the proposed setup with two optical cavities. Section II C discusses the optical matrix element due to the e-ph interaction between a qubit electron and a cavity photon. In Sec. II D, we describe the photon-valley QST in the two-cavity setup. The discussion of QST here intends to provide a qualitative picture of the process, by giving the initial, intermediate, and final states involved, in preparation for the discussion of a more complete quantum-mechanical treatment in Sec. III.

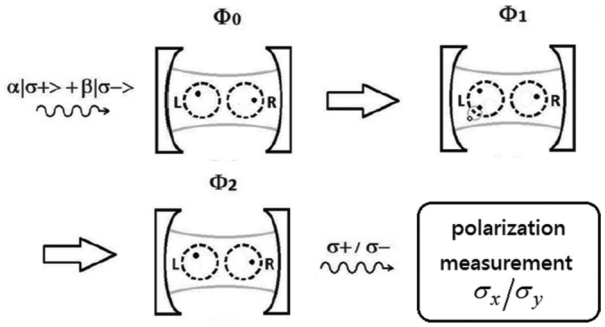

FIG. 2. The QST from a photon qubit to a valley-pair qubit in an optical cavity. Dashed circles: quantum dots; black/hollow dots: electrons/holes.

A. The QST with one cavity

The principle underlying the valley-photon QST is the unique, approximate valley-polarization correspondence mentioned earlier, which enables a natural QST between valley and photon qubits. Figure 2 shows a simple, conceptual setup for the QST, where the photon enters an optical cavity, interacts with the valley qubit placed inside, and leaves the cavity. Illustration of the concept of valley-photon QST is given below within this setup.

The photon to valley QST is featured by

(i) initialization of the valley qubit into the singlet state $\frac{1}{\sqrt{2}}(|K_{\rm L}K'_{\rm R}\rangle - |K'_{\rm L}K_{\rm R}\rangle)$;

(ii) the incoming signal photon of energy $\hbar\omega_{\rm ph}$ in a generic state $\alpha|\sigma_+\rangle + \beta|\sigma_-\rangle$ of mixed circular polarizations ($\sigma+$ and $\sigma-$) that carries the quantum information in $\{\alpha,\beta\}$;

(iii) enhancement of the e-ph interaction in the cavity;

(iv) gate tuning of energy levels in one of the two QDs (taken to be QDL, the left QD, throughout the paper) to achieve the trion-generating or -eliminating resonant transitions $\hbar\omega_{\rm ph} + |K_{\rm L}\rangle \leftrightarrow |K'_{\rm eh,L}K_{\rm L}\rangle$ and $\hbar\omega_{\rm ph} + |K'_{\rm L}\rangle \leftrightarrow |K_{\rm eh,L}K'_{\rm L}\rangle$ in QDL, where $|K'_{\rm eh,L}K_{\rm L}\rangle$ is the trion consisting of one K electron, one K' electron, and one K' hole, for example;

(v) gate control to switch off the tunneling coupling between the QDs and to freeze the inter-QD orbital motion, thus eliminating the electron in QDR (the right QD) from our consideration of the QST process, except for its entanglement with the electron in QDL; and

(vi) linear polarization (σx and σy) state projection measurement of the valley qubit-emitted photon.

In the ideal case where the valley-polarization correspondence is exact, the QST proceeds in the following

sequence [26]:

$$|\Phi_0\rangle = \frac{1}{\sqrt{2}}(|K_{\rm L}K'_{\rm R}\rangle - |K'_{\rm L}K_{\rm R}\rangle)\otimes(\alpha|\sigma_+\rangle + \beta|\sigma_-\rangle)$$

$$\overset{\text{photon absorption}}{\rightarrow} |\Phi_1\rangle = \frac{1}{\sqrt{2}}(\beta|K'_{\rm ex,L}K_{\rm L}K'_{\rm R}\rangle - \alpha|K_{\rm ex,L}K'_{\rm L}K_{\rm R}\rangle)$$

$$\overset{\text{photon emission/absorption}}{\leftrightarrow} |\Phi_2\rangle = \beta|K_{\rm L}K'_{\rm R}\rangle\otimes|\sigma_-\rangle - \alpha|K'_{\rm L}K_{\rm R}\rangle\otimes|\sigma_+\rangle$$

$$\overset{\text{projection onto } \sigma_x/\sigma_y}{\rightarrow} |\Phi_{3x}\rangle = \beta|K_{\rm L}K'_{\rm R}\rangle - \alpha|K'_{\rm L}K_{\rm R}\rangle(\text{if } \sigma_x\text{detected})|\Phi_{3y}\rangle = \beta|K_{\rm L}K'_{\rm R}\rangle + \alpha|K'_{\rm L}K_{\rm R}\rangle(\text{if } \sigma_y\text{detected})$$

Note that in the intermediate state $|\Phi_2\rangle$, the photon and the qubit electrons are entangled. The electrons now share the quantum information carried in the amplitudes $\{\alpha,\beta\}$. The entangled photon eventually leaks out of the cavity, and a σ_x/σ_y projection measurement is performed on its linear polarization state. The projection unentangles the photonic component, leaving the information solely stored in the valley-pair state (Φ_{3x} or Φ_{3y}). If desired, the resultant valley state could be further transformed by standard single qubit manipulations into the combination of valley singlet and triplet states, for example,

$$\beta|K_{\rm L}K'_{\rm R}\rangle - \alpha|K'_{\rm L}K_{\rm R}\rangle \rightarrow \alpha\frac{1}{\sqrt{2}}(|K_{\rm L}K'_{\rm R}\rangle - |K'_{\rm L}K_{\rm R}\rangle) + \beta\frac{1}{\sqrt{2}}(|K_{\rm L}K'_{\rm R}\rangle + |K'_{\rm L}K_{\rm R}\rangle),$$

thus storing $\{\alpha,\beta\}$ in the robust, decoherence-free valley state.

We note that the existence of bound states of excitons and trions are not required for the valley-photon QST. The terminology of trions is used in our paper just to indicate the presence in the QST of intermediate states consisting of two electrons and one hole with Coulomb interaction among them.

The reverse process of valley to photon QST can be similarly achieved. We replace the initial state by

$$|\Phi_0\rangle = (\beta|K_{\rm L}K'_{\rm R}\rangle - \alpha|K'_{\rm L}K_{\rm R}\rangle)\otimes\frac{1}{\sqrt{2}}(|\sigma_+\rangle + |\sigma_-\rangle),$$

with the quantum information $\{\alpha,\beta\}$ now encoded into the valley-pair qubit. The interqubit interaction leads next to the following state evolution:

$$\overset{\text{photon absorption}}{\rightarrow} |\Phi_1\rangle = \frac{1}{\sqrt{2}}(\beta|K'_{\rm ex,L}K_{\rm L}K'_{\rm R}\rangle - \alpha|K_{\rm ex,L}K'_{\rm L}K_{\rm R}\rangle)$$

$$\overset{\text{photon emission/absorption}}{\leftrightarrow} |\Phi_2\rangle = \beta|K_{\rm L}K'_{\rm R}\rangle\otimes|\sigma_-\rangle - \alpha|K'_{\rm L}K_{\rm R}\rangle\otimes|\sigma_+\rangle.$$

Now, instead of measuring the photon, we measure the valley qubit and project it onto singlet/triplet states:

$$\overset{\text{projection onto } Z_S/Z_{T0}}{\rightarrow} |\Phi_{3S}\rangle \equiv \alpha|\sigma_+\rangle + \beta|\sigma_-\rangle \text{ (if } Z_S \text{ detected)}$$

$$|\Phi_{3T_0}\rangle \equiv -\alpha|\sigma_+\rangle + \beta|\sigma_-\rangle \text{ (if } Z_{T_0} \text{ detected)},$$

which completes the transfer by storing $\{\alpha,\beta\}$ in the photon states Φ_{3S} or Φ_{3T_0}.

From now on, our investigation will focus on the photon to valley QST, the process actually used in a QR.

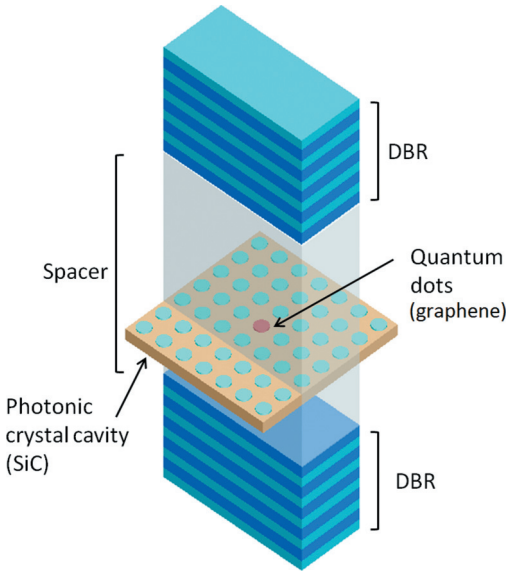

FIG. 3. The proposed hybrid-cavity setup. The valley-pair qubit (red dot in the middle plane) is placed at the center of the PC cavity. It is also vertically confined by the cavity formed with DBRs on both top and bottom sides. The signal photon comes in through the top DBR and excites a trion in QD_L, which later radiates a photon moving out of the PC cavity in a nearly horizontal direction into a photon sensor.

B. Setup with two cavities

An issue with the single cavity setup in Fig. 2 lies in the existence of a finite probability for the incoming photon to enter the cavity, to leak out of the cavity, and to enter the polarization projection measurement, without ever interacting and becoming entangled with the electron. Since the e-ph entanglement is a necessary condition for a successful QST, a detection of the idler photon would create a false event of QST and, hence, reduce the fidelity. It is therefore desirable to resolve the overlap between the idling and the entangled photons. This could be done in either the spatial or the frequency domains. In this paper, we consider a configuration involving two optical cavities with orthogonal cavity axes: One gives vertical (z) optical confinement and the other transverse (x-y) optical confinement, as shown in Fig. 3, with the qubit sitting at the center of both cavities. The configuration effects an enhancement of the e-ph interaction as well as a differentiation between the paths of incoming and outgoing signal photons, as follows. The first cavity is formed of a pair of DBRs that provide the vertical confinement. It couples a vertically incoming signal photon into a DBR cavity mode and excites a trion in QD_L. On the other hand, for the transverse confinement, we envision a defect in a 2D PC of square lattice structure, as shown in Fig, 3, with the qubit placed at the center of the defect. The defect forms a cavity with partially confined transverse electric (TE) modes. These PC cavity modes have electric fields and wave vectors lying in the plane [42–44]

and hence are efficiently e-ph coupled to a QD_L electron in the graphene plane. The coupling induces the trion to emit a photon into a PC cavity mode, which eventually leaks out of the cavity in a nearly in-plane direction and can be picked up by a sensor. Once detected, the photon becomes disentangled from the valley qubit, and this completes the state transfer.

C. Optical matrix elements

Throughout the paper, we take the valley qubit to be embedded in a gapped monolayer graphene (e.g., BN-doped monolayer graphene [45]) such that we can use the simple 2D Dirac theory of monolayer graphene [11,13] in the modeling in order to simplify the analysis while retaining the essential valley physics. For the QST, we consider the interaction between a QD_L electron and a radiation field of frequency ω_{ph}. The electron in QD_L is governed by the following 2D Dirac equation [13]

$$\begin{aligned}
&\left(H_D^{(0)}+H_A\right)\phi_D = i\hbar\partial_t\phi_D,\\
&H_D^{(0)} = \begin{pmatrix}\Delta(\vec{r})+V(\vec{r}) & v_F\hat{p}_-\\ v_F\hat{p}_+ & -\Delta(\vec{r})+V(\vec{r})\end{pmatrix},\\
&H_A = \begin{pmatrix}0 & ev_FA_-\\ ev_FA_+ & 0\end{pmatrix},\quad \phi_D=\begin{pmatrix}\varphi_A\\ \varphi_B\end{pmatrix},\\
&A_\pm = A_x \pm i\tau_v A_y,\\
&\hat{p}_\pm = p_x \pm i\tau_v p_y = -i\partial_x \pm \tau_v\partial_y.
\end{aligned}\tag{1}$$

Here, H_A is the e-ph interaction between the electron and the radiation field, with $\vec{A}=(A_x,A_y)$ being the in-plane vector potential of the field. $H_D^{(0)}$ is the QD_L Hamiltonian in the absence of radiation, with $\delta(\vec{r})$ and $V(\vec{r})$ being, respectively, the band gap profile and the potential energy profile that give rise to the QD confinement. Let $\phi_D^{(0,c)}$ and $\phi_D^{(0,v)}$ denote the confined states with corresponding energies $E_0^{(c)}$ and $E_0^{(v)}$, respectively. Specifically, they are respectively the lowest conduction band and highest valence band eigenstates of $H_D^{(0)}$ given by

$$\begin{aligned}
\phi_D^{(0,c)} &= \begin{cases}\begin{pmatrix}\varphi_{A,>}^{(0,c)}\\ \varphi_{B,<}^{(0,c)}\end{pmatrix}, \tau_v=+1\\ \begin{pmatrix}\varphi_{A,>}^{(0,c)}\\ -\varphi_{B,<}^{(0,c)}\end{pmatrix}^*, \tau_v=-1\end{cases},\\
\phi_D^{(0,v)} &= \begin{cases}\begin{pmatrix}\varphi_{A,<}^{(0,v)}\\ \varphi_{B,>}^{(0,v)}\end{pmatrix}, \tau_v=+1\\ \begin{pmatrix}\varphi_{A,<}^{(0,v)}\\ -\varphi_{B,>}^{(0,v)}\end{pmatrix}^*, \tau_v=-1\end{cases},
\end{aligned}\tag{2}$$

where the subscripts A and B denote the two atomic sites in a graphene unit cell. We take the above QD ground states to be near band edges; therefore, $\varphi_{B,<}^{(0,c)} \approx v_F\hat{p}_+\varphi_{A,>}^{(0,c)}/2\Delta \ll ||\varphi_{A,>}^{(0,c)}||$ and $\varphi_{A,<}^{(0,v)} \approx -v_F\hat{p}_-\varphi_{B,>}^{(0,v)}/2\Delta \ll ||\varphi_{B,>}^{(0,v)}||$. The states with $\tau_v=1$ and $\tau_v=-1$ are related by time reversal symmetry and are basically complex conjugates of each other as given above. Near resonance ($\omega_{ph}\approx E_0^{(c)}-E_0^{(v)}$), the optical response is governed by the optical matrix element $M \equiv \langle\phi_D^{(0,c)}|H_A|\phi_D^{(0,v)}\rangle$. Below, we analyze M, with the radiation field representing either a DBR or PC cavity photon.

We start with the DBR cavity (DC) mode. In typical applications, the mode has a wave length much greater than the size of the qubit QDs. Therefore, we take its electric field inside QD_L to be approximately constant, with the in-plane component $\vec{E}_0=\vec{E}_{DC}(\vec{r}=0,z=0)$ and the corresponding in-plane vector potential $\vec{A}=\frac{\vec{E}_0}{i\omega_{ph}}e^{-i\omega_{ph}t}$. Here, we take the graphene plane to be located at $z=0$, and QD_L at $\vec{r}\equiv(x,y)=0$ of the plane. Below we list the matrix elements for various combinations of $\vec{E}_0$ polarization and valley pseudospin ($E_0=|\vec{E}_0|$):

$$\begin{aligned}
M_> &= ev_F\langle\varphi_{A,>}^{(0,c)}| - \frac{iE_0}{\omega_{ph}}|\varphi_{B,>}^{(0,v)}\rangle \quad \text{for } (\sigma_+,K)\\
M_< &= ev_F\langle\varphi_{B,<}^{(0,c)}| - \frac{iE_0}{\omega_{ph}}|\varphi_{A,<}^{(0,v)}\rangle \quad \text{for } (\sigma_-,K)\\
-M_<{}^* &= ev_F\langle\varphi_{B,<}^{(0,c)*}| - \frac{iE_0}{\omega_{ph}}|\varphi_{A,<}^{(0,v)*}\rangle \quad \text{for } (\sigma_+,K')\\
-M_>{}^* &= ev_F\langle\varphi_{A,>}^{(0,c)*}| - \frac{iE_0}{\omega_{ph}}|\varphi_{B,>}^{(0,v)*}\rangle \quad \text{for } (\sigma_-,K')
\end{aligned}\tag{3}$$

In the above, (σ_+,K) denotes the absorption of a σ_+ polarized photon by a K valence electron in QD_L, for example. Basically, for near band edge states, because $|\phi_>| \gg |\phi_<|$, it gives $|M_>| \gg |M_<|$. If we totally ignore the minor matrix element $M_<$, then Eq. (3) yields, for optical excitation, the major matrix element $M_>$ consistent with the valley-polarization correspondence in Fig. 1. However, since $M_<$ is finite, the correspondence is only approximate. After substituting $\varphi_{B,<}^{(0,c)} \approx v_F\hat{p}_+\varphi_{A,>}^{(0,c)}/2\Delta$ and $\varphi_{A,<}^{(0,v)} \approx -v_F\hat{p}_-\varphi_{B,>}^{(0,v)}/2\Delta$ into $M_<$, we obtain

$$\begin{aligned}
M_< &\approx ev_F\left\langle\frac{1}{2\Delta}v_F\hat{p}_+\varphi_{A,>}^{(0,c)}\right| - \frac{iE_0}{\omega_{ph}}\left|\frac{1}{-2\Delta}v_F\hat{p}_-\varphi_{B,>}^{(0,v)}\right\rangle \quad \text{for } (\sigma_-,K)\\
M_<{}^* &\approx ev_F\left\langle\frac{1}{2\Delta}v_F\hat{p}_-\varphi_{A,>}^{(0,c)*}\right| - \frac{iE_0}{\omega_{ph}}\left|\frac{1}{-2\Delta}v_F\hat{p}_+\varphi_{B,>}^{(0,v)*}\right\rangle \quad \text{for } (\sigma_+,K')
\end{aligned}\tag{4}$$

The above expressions are useful for the estimation of the parameters $M_>$ and $M_<$ in our numerical investigation of the QST. In general, the ratio $M_</M_>$ depends on the QD geometry as well as the confinement. For example, in a QD with electron-hole symmetry, Eqs. (3) and (4) imply that $M_</M_> \propto \langle\hat{p}_+\varphi_{A,>}^{(0,c)} \mid \hat{p}_-\varphi_{A,>}^{(0,c)}\rangle \approx \langle k_x^2-k_y^2-2ik_xk_y\rangle$. In the case of a circular disk QD, $\langle k_x^2-k_y^2\rangle=\langle k_xk_y\rangle=0$, so $M_<=0$, while in an elliptic QD, $\langle k_xk_y\rangle$ vanishes and so does the imaginary part of $M_<$. For a generic, asymmetric QD, $\langle k_xk_y\rangle$ is likely to be finite, so $M_<$ generally carries a phase relative to $M_>$. Last, we note that the above discussion of matrix elements has been performed within the one-electron picture. As such, for trion-involved optical transitions considered in the study, the expressions of matrix elements will be modified by many-electron effects. However, since the primary key to the photon-valley QST—the relations among the various

matrix elements in Eqs. (3) and (4)—is established only on the basis of the time reversal symmetry relating the two states of opposite pseudospins, its validity holds even in the presence of many-electron effects, as briefly explained below. Consider the trion in QD_L with one K electron, one K hole, and one K' electron. In the presence of Coulomb interaction, the trion wave function is given by [46]

$$\Psi^{(K)}_{\text{trion}} = \sum_{k_e,k_h,k'_e} c(k_e,k_h,k_e')|k_e+K,k_h+K,k'_e+K'\rangle.$$

A similar expression holds for $\Psi^{(K')}_{\text{trion}}$. Here, $|k_e+K,k_h+K,k'_e+K'\rangle$ is a basis state consisting of two free electrons and one hole, with corresponding wave vectors as specified in the ket, and $c(k_e,k_h,k'_e)$ is the corresponding expansion coefficient. Distinct basis states are coupled together by the electron-electron and electron-hole Coulomb interaction as well as the QD confinement potential, giving the trion state as a linear combination of these basis states. This generalizes the final state in optical absorption considered in Eq. (3) from a free conduction band electron in one-electron picture to the corresponding trion in many-electron picture. Moreover, let H_{trion} denote the corresponding trion Hamiltonian. Due to the time reversal symmetry between K and K', it follows that [46]

$$H_{\text{trion}}\Psi^{(K)}_{\text{trion}} = E\Psi^{(K)}_{\text{trion}} H_{\text{trion}}\Psi^{(K')}_{\text{trion}} = E\Psi^{(K')}_{\text{trion}},$$
$$\Psi^{(K')}_{\text{trion}} = \left(\Psi^{(K)}_{\text{trion}}\right)^*,$$

which generalizes the final state identity from $\varphi^{(0,c)}_{A,>} = (\varphi^{(0,c)*}_{A,>})^*, \varphi^{(0,c)}_{B,<} = (\varphi^{(0,c)*}_{B,<})^*$ in Eq. (3) to $\Psi^{(K')}_{\text{trion}} = \Psi^{(K)*}_{\text{trion}}$. Since the relations among the various matrix elements in Eq. (3) depend only on such final state identities, we conclude that in the presence of many-electron effects the same relations continue to hold and many-electron effects only modify the matrix elements in magnitude. This modification in magnitude is covered in our paper by giving the matrix elements a range of magnitudes and studying the QST as a function of these magnitudes. Therefore, while one-electron expressions in Eqs. (3) and (4) will be used below for numerical estimation of the matrix elements, by adopting the foregoing approach our paper does not depend so much on the validity of one-electron approximation and actually allows the paper to go beyond the approximation.

Next, we discuss the optical matrix element involving the PC cavity mode. We take the mode to be a TE donor type state at X point, for example, one that transforms according to the symmetry of 2D E representation of C_{4v}, i.e., the symmetry group of a square [47]. There are two degenerate modes in the representation as follows. Let $H_{\text{PC}}(\vec{\text{r}})\hat{z}$ and $\vec{E}_{\text{PC}}(\vec{\text{r}})$ denote the H-field and E-field of the modes in the graphene plane, respectively ($\hat{z}$ = unit vector normal to the plane). Then, $H_{\text{PC}}(\vec{\text{r}})$ transforms as $\sin(\vec{k}_{X_1}\cdot\vec{\text{r}})$ or $\sin(\vec{k}_{X_2}\cdot\vec{\text{r}})$, and $\vec{E}_{\text{PC}}(\vec{\text{r}}) = \frac{1}{-i\omega_{\text{ph}}\mu_0\varepsilon(\vec{\text{r}})}\nabla\times H_{\text{PC}}(\vec{\text{r}})\hat{z}$ transforms as $\hat{z}\times\vec{k}_{X_1}\cos(\vec{k}_{X_1}\cdot\vec{\text{r}})$ or $\hat{z}\times\vec{k}_{X_2}\cos(\vec{k}_{X_2}\cdot\vec{\text{r}})$. Here $\{\vec{k}_{X_1}, \vec{k}_{X_2}\}$ are the two orthogonal wave vectors at X points of the Brillouin zone, μ_0 = vacuum magnetic permeability, and ε = dielectric constant. Note that at $\vec{\text{r}}=0$ (center of the cavity) where the qubit is located, $\vec{E}_{\text{PC}}(\vec{\text{r}})$s of the two modes are $\{\sigma_x,\sigma_y\}$ polarized, in a way correlated to their propagation directions $\{\vec{k}_{X_1}, \vec{k}_{X_2}\}$. For the optical matrix elements, we can linearly combine the two modes, making it either σ_+ or σ_- polarized at $\vec{\text{r}}=0$, and continue using the same expressions in Eq. (3) with $\vec{E}_0$ replaced by $\vec{E}_{\text{PC}}(\vec{\text{r}}=0)$. Effectively, this means that the matrix elements for the PC cavity are scaled from those for the DBR cavity by the factor $|\vec{E}_{\text{PC}}(\vec{\text{r}}=0)/\vec{E}_0|$. In particular, it follows that the major matrix elements for the two cavities carry the same phase and so do the minor ones.

Equations (3) and (4) are used to estimate the matrix elements for the numerical study in Sec. IV. As an example, we take $\omega_{\text{ph}} = 1.6\cdot10^5$ GHz corresponding to a graphene band gap of 0.1 eV, and the modal volumes to be $V_{\text{mode}} = 10^4\,\mu\text{m}^3$ for the DBR cavity and $V_{\text{mode}} = 600$ for the PC cavity. As a reference, we also list $(\lambda/n)^3 = 1600\,\mu\text{m}^3$ for the DBR cavity with the index of refraction n taken to be 1 (for air), and $(\lambda/n)^3 = 94\,\mu\text{m}^3$ for the PC cavity with n taken to be 2.6 (in the case of SiC), respectively, where λ is the photon wave length in vacuum. We take the QD to be a square well with edge length of 70 nm and subject to hard wall confinement. This gives the electron velocity $v = 0.4v_{\text{F}}$ in the QD, where v_F (the Fermi velocity) is taken to be 10^6 m/sec. Using the above numbers along with the approximations $\langle\varphi^{(0,c)}_{A,>}|E_0|\varphi^{(0,v)}_{B,>}\rangle \approx E_0$ and $E_0 \sim \sqrt{\hbar/4\pi\varepsilon\omega_{\text{ph}}V_{\text{mode}}}$ in Eq. (3), we obtain $|M_>| \sim$ 30 GHz for the DBR cavity and 45 GHz for the PC cavity. Moreover, using the approximation $|M_<| \sim \frac{v^2}{4v_F^2}|M_>|$ for Eq. (4), we obtain $|M_</M_>| = 0.04$. The ratio holds for both cavities since the matrix elements in the two cases are given by the same forms of expressions in Eqs. (3) and (4).

In the following discussion, we introduce the notations $\{A, B\}$ and $\{C, D\}$ to represent $\{M_>, M_<\}$ for the PC and DBR cavity modes, respectively, with $B/A = D/C$. In addition, as it will become obvious below in Sec. II D, only the relative phase between $M_>$ and $M_<$ matters in the QST, so we take $M_>$ (A and C) to be real numbers and place the relative phase in $M_<$ (B and D), which allows us to write, for example, $B = A|B/A|e^{i\phi_{B/A}}$. Generally, in a favorable configuration design for the QST, a correlation between A and C would be required so that the design can move the QST process forward to the finish line with a good yield. More details will be given in the following sections.

D. The QST with two cavities

We examine the QST in the setup with two cavities. In the presence of finite B and D, the various states involved in the QST are modified from those in Sec. II A, giving

$$|\Phi_0\rangle = \frac{1}{\sqrt{2}}(|K_{\text{L}}K'_{\text{R}}\rangle - |K'_{\text{L}}K_{\text{R}}\rangle)\otimes(\alpha|\sigma_+\rangle + \beta|\sigma_-\rangle),$$
$$|\Phi_1\rangle \propto (-\beta C^* + \alpha D)|K'_{\text{ex,L}}K_{\text{L}}K'_{\text{R}}\rangle - (\alpha C - \beta D^*)|K_{\text{ex,L}}K'_{\text{L}}K_{\text{R}}\rangle,$$
$$|\Phi_2\rangle = \text{valley-polarization entangled stateafter photon emission from the trion}$$
$$\propto (-\beta C^* + \alpha D)(-A|\sigma_-\rangle\otimes|K_{\text{L}}K'_{\text{R}}\rangle + B^*|\sigma_+\rangle\otimes|K_{\text{L}}K'_{\text{R}}\rangle) - (\alpha C - \beta D^*)(A^*|\sigma_+\rangle\otimes|K'_{\text{L}}K_{\text{R}}\rangle - B|\sigma_-\rangle\otimes|K'_{\text{L}}K_{\text{R}}\rangle),$$

$$|\Phi_{3x}\rangle \propto (-\beta C^* + \alpha D)(-A + B^*)|K_L K'_R\rangle - (\alpha C - \beta D^*)(A^* - B)|K'_L K_R\rangle,$$
$$|\Phi_{3y}\rangle \propto (\beta C^* - \alpha D)(A + B^*)|K_L K'_R\rangle + (\alpha C - \beta D^*)(A^* + B)|K'_L K_R\rangle. \quad (5)$$

We note several points. First, the emergence of matrix elements A, B, C, and D in Eq. (5) indicates the presence of two cavities. Second, with two cavities, the photon in the entangled state $|\Phi_2\rangle$ leaks out of the PC cavity via TE modes. For these modes, as their polarizations $\{\sigma_x,\sigma_y\}$ are correlated to the propagation directions $\{\vec{k}_{X_1},\vec{k}_{X_2}\}$, a detection of the photon's outgoing direction effects the projection of $|\Phi_2\rangle$ onto $|\Phi_{3x}\rangle$ or $|\Phi_{3y}\rangle$. Last, if we set the minor optical matrix elements $B = D = 0$, then the final states are given by $|\Phi_{3x}\rangle \propto \beta|K_L K'_R\rangle - \alpha|K'_L K_R\rangle$ or $|\Phi_{3y}\rangle \propto \beta|K_L K'_R\rangle + \alpha|K'_L K_R\rangle$ with the same amplitudes α and β that are encoded into the incoming photon, meaning that no distortion occurs in the QST process. We thus define the entangled state with $B = D = 0$ as

$$|\Psi_{\text{ideal}}\rangle \equiv \frac{1}{\sqrt{2}}[(\beta|K_L K'_R\rangle - \alpha|K'_L K_R\rangle) \otimes |\sigma_x\rangle - i(\beta|K_L K'_R\rangle + \alpha|K'_L K_R\rangle) \otimes |\sigma_y\rangle], \quad (6)$$

which serves as a reference state for the definition of fidelity. For example, if we ignore any cavity leakage and qubit decoherence, the fidelity would then be given by $F = N_2|\langle\Psi_{\text{ideal}}|\Phi_2\rangle|$, with a value less than unity since small yet finite B and D would create in $|\Phi_2\rangle$ a deviation from $|\Psi_{\text{ideal}}\rangle$ (N_2 = the normalization constant of $|\Phi_2\rangle$). Section III treats the general case where both the cavity leakage and intermediate state damping are present.

III. THEORETICAL MODEL

In a realistic system, the QST depends on various parameters of the configuration in which the QST takes place, such as optical transition matrix elements, various decoherence times, and Q factors of cavities. In Sec. III A, we provide a quantum-mechanical description of the realistic QST problem. In Sec. III B, we discuss the wave equation and solution and then derive the yield and fidelity.

A. Description of the problem

For a quantum-mechanical description of QST in the setup of Fig. 3, we refer to the following process flow diagram:

In Fig. 4, the incoming signal photon injects into the DBR cavity with the tunneling coupling given by κ_k. Next, the cavity photon is absorbed exciting a trion in QD_L, with the major (minor) coupling given by C (D) between the trion and the DBR cavity mode. The trion then radiates a photon into the PC cavity mode, with the major (minor) coupling given by A (B) between the trion and the PC cavity mode. Last, the photon leaks out of the PC cavity with the coupling constant given by T_k and enters a photon sensor. The parameter $2\kappa_{DC}$ is the leakage rate of DBR cavity mode, and $2\gamma_{SE}$ is the decay rate of trion accounting for its nonradiative decay as well as emission into modes excluding the DBR and PC cavity ones. Note that we assume that the coupling between the DRB and PC cavities is negligible because of the significant mode mismatch between them.

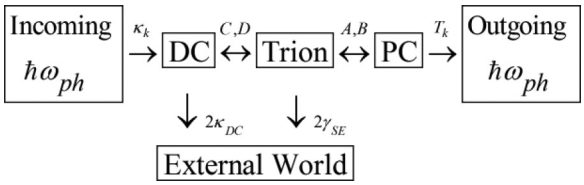

FIG. 4. The process flow diagram. The DC denotes the DBR cavity mode, and PC denotes the PC cavity mode. The various parameters shown in the diagram are the couplings and decay or leakage rates involved in the flow from one stage to the next, as explained in the text.

The quantum-mechanical system involved consists of electrons, trions, cavity photons, incoming and outgoing photons, and the interaction among them. Below we discuss the state vector, Hamiltonian, wave equation, and, finally, the solution to the equation.

The total state vector describes an e-ph composite system and is given by

$$|\Psi(t)\rangle = \sum_{\sigma=\sigma_+,\sigma_-;\tau=K,K'} \int dx \phi^{\text{input}}_{\sigma\tau}(x,t)|\tau'_L,\tau_R\rangle \otimes |x,\sigma\rangle + \sum_{\sigma=\sigma_+,\sigma_-;\tau=K,K'} \phi^{\text{DC}}_{\sigma\tau}(t)|\tau'_L,\tau_R\rangle \otimes |\text{DC},\sigma\rangle + \sum_{\tau=K,K'} \phi^{\text{trion}}_{\tau}(t)|\tau_{\text{ex,L}},\tau'_L,\tau_R\rangle + \sum_{\sigma=\sigma_+,\sigma_-;\tau=K,K'} \phi^{\text{PC}}_{\sigma\tau}(t)|\tau'_L,\tau_R\rangle \otimes |\text{PC},\sigma\rangle + \sum_{\sigma=\sigma_+,\sigma_-;\tau=K,K';k_{2D}} \phi^{\text{output}}_{\sigma\tau}(k_{2D},t)|\tau'_L,\tau_R\rangle \otimes |k_{2D},\sigma\rangle. \quad (7)$$

In the above expression, we define $\tau' = K(K')$ for $\tau = K'(K)$. $|\tau'_L,\tau_R\rangle$ denotes the two-electron state with the QDL electron in the τ'_L valley and the QDR electron in the opposite τ_R valley; $|x,\sigma\rangle$ denotes the incoming signal photon state with position x and circular polarization σ; $|\text{DC},\sigma\rangle$ denotes a DBR cavity mode with polarization σ at the qubit; $|\tau_{\text{ex,L}},\tau'_L,\tau_R\rangle$ denotes a trion-electron state, with the trion (specified by $\tau_{\text{ex,L}},\tau'_L,\tau_R$) in QDL and the electron (specified by τ_R) in QDR; $|\text{PC},\sigma\rangle$ denotes a PC cavity mode with polarization σ at the qubit; and $|k_{2D},\sigma\rangle$ denotes an outgoing signal photon state moving to the photon sensor with a planar wave vector k_{2D} and polarization σ. $\phi^{\text{input}}_{\sigma\tau}$, $\phi^{\text{DC}}_{\sigma\tau}$, $\phi^{\text{trion}}_{\tau}$, $\phi^{\text{PC}}_{\sigma\tau}$, and $\phi^{\text{output}}_{\sigma\tau}$ are the amplitudes of various basis states and governed by the corresponding wave equation (see Sec. III B). $\phi^{\text{input}}_{\sigma\tau}$ is used as an input to the equation. The 14 amplitudes $\{\phi^{\text{DC}}_{\sigma\tau}$, $\phi^{\text{trion}}_{\tau}$, $\phi^{\text{PC}}_{\sigma\tau}$, $\phi^{\text{output}}_{\sigma\tau}$ for $\sigma = \sigma_+,\sigma_-$ and $\tau = K,K'\}$ are determined by solving the equation. $\phi^{\text{output}}_{\sigma\tau}$ describes the output from the system, and, once solved, it is used to determine both the yield and fidelity.

In the input to the system, the e-ph system is treated as an open system with both input from and output to the external world. In particular, in the corresponding wave equation, the

input is prescribed in advance as a time-dependent boundary condition. In details, the incoming photonic signal is taken to be a Gaussian wave packet, and, together with the initial singlet state of the valley qubit, it leads to the following product state as the input to the e-ph system:

$$|\Phi^{\text{input}}\rangle = G(t)(\alpha|\sigma_+\rangle + \beta|\sigma_-\rangle) \otimes \frac{1}{\sqrt{2}}(|K_{\text{L}}K'_{\text{R}}\rangle - |K'_{\text{L}}K_{\text{R}}\rangle), \tag{8}$$

where $G(t) \propto \phi^{\text{input}}_{\sigma\tau}(x=0,t)$ denotes the Gaussian wave packet evaluated at the DBR cavity-environment interface the incoming photon hits upon, with the interface taken to be located at $x = 0$. Specifically, it is given by

$$G(t) = \int_{-\infty}^{\infty} \frac{d\omega}{2\pi}\phi_0^{\text{ph}}\sqrt{L}e^{-i(\omega-\omega_{\text{ph}})x_0/c}e^{-(\omega-\omega_{\text{ph}})^2/2\Delta\omega_{\text{ph}}^2}e^{-i\omega t},$$
$$\phi_0^{\text{ph}} \equiv \pi^{\frac{1}{4}}\sqrt{\frac{2}{c\Delta\omega_{\text{ph}}}}, \tag{9}$$

with x_0 being the initial center of the wave packet at $t = 0$, $\Delta\omega_{\text{ph}}$ being the band width, L being the size of the external world, and c being the speed of light. The wave packet above has been taken to be primarily composed of waves normally incident upon the DBR. Expanding the product, we obtain the four components of $|\Phi^{\text{input}}\rangle$ as

$$|\phi^{\text{input}}\rangle = \left(\phi^{\text{input}}_{\sigma_+,K}(t),\phi^{\text{input}}_{\sigma_-,K}(t),\phi^{\text{input}}_{\sigma_+,K'}(t),\phi^{\text{input}}_{\sigma_-,K'}(t)\right)^T$$
$$= 1/\sqrt{2}(-\alpha G(t), -\beta G(t),\alpha G(t),\beta G(t))^T \tag{10}$$

which are inputs to the wave equation discussed later.

The Hamiltonian of the e-ph system is given by

$$H = H_{\text{input}} + H_{\text{DC}} + H_{\text{trion}} + H_{\text{PC}} + H_{\text{output}} + H_{\text{reservoir}} + H_{\text{input-DC}} + H_{\text{DC-trion}} + H_{\text{trion-PC}} + H_{\text{PC-output}} + H_{SE}. \tag{11}$$

The various terms are given as follows ($\hbar = 1$):

$$H_{\text{input}} = \sum_{\substack{\sigma=\sigma_+,\sigma_-;\\ \tau=K,K';\\ k_{1\text{D}}}} c|k_{1\text{D}}||\tau'_{\text{L}}\tau_{\text{R}}\rangle \otimes |k_{1\text{D}},\sigma\rangle\langle k_{1\text{D}},\sigma| \otimes \langle\tau'_{\text{L}}\tau_{\text{R}}|,$$

$$H_{\text{DC}} = \sum_{\sigma=\sigma_+,\sigma_-;\tau=K,K'} \omega_{\text{DC}}|\tau'_{\text{L}}\tau_{\text{R}}\rangle \otimes |\text{DC},\sigma\rangle\langle\text{DC},\sigma| \otimes \langle\tau'_{\text{L}}\tau_{\text{R}}|,$$

$$H_{\text{trion}} = \sum_{\sigma=\sigma_+,\sigma_-;\tau=K,K'} \omega_{\text{trion}}|\tau_{\text{ex,L}}\tau'_{\text{L}}\tau_{\text{R}}\rangle\langle\tau_{\text{ex,L}}\tau'_{\text{L}}\tau_{\text{R}}|,$$

$$H_{\text{PC}} = \sum_{\sigma=\sigma_+,\sigma_-;\tau=K,K'} \omega_{\text{PC}}|\tau'_{\text{L}}\tau_{\text{R}}\rangle \otimes |\text{PC},\sigma\rangle\langle\tau'_{\text{L}}\tau_{\text{R}}| \otimes \langle\text{PC},\sigma|,$$

$$H_{\text{output}} = \sum_{\substack{\sigma=\sigma_+,\sigma_-;\\ \tau=K,K';\\ \vec{k}_{2\text{D}}}} c|\vec{k}_{2\text{D}}||\tau'_{\text{L}}\tau_{\text{R}}\rangle \otimes |\overrightarrow{k}_{2\text{D}},\sigma\rangle\langle\tau'_{\text{L}}\tau_{\text{R}}| \otimes \langle\overrightarrow{k}_{2\text{D}},\sigma|,$$

$$H_{\text{reservoir}} = \sum_{\sigma=\sigma_+,\sigma_-;\tau=K,K';\mu} \omega_\mu|\tau'_{\text{L}}\tau_{\text{R}}\rangle \otimes |\mu,\sigma\rangle\langle\mu,\sigma| \otimes \langle\tau'_{\text{L}}\tau_{\text{R}}|,$$

$$H_{\text{input-DC}} = \sum_{\substack{\sigma=\sigma_+,\sigma_-;\\ \tau=K,K';\\ k_{1\text{D}}}} (\kappa_k|\tau'_{\text{L}}\tau_{\text{R}}\rangle \otimes |\text{DC},\sigma\rangle\langle\tau'_{\text{L}}\tau_{\text{R}}| \otimes \langle k_{1\text{D}},\sigma| + \text{h.c.}),$$

$$H_{\text{trion-PC}} = A|K_{\text{ex,L}}K'_{\text{L}}K_{\text{R}}\rangle\langle K'_{\text{L}}K_{\text{R}}| \otimes \langle\text{PC},\sigma_+| + B|K_{\text{ex,L}}K'_{\text{L}}K_{\text{R}}\rangle\langle K'_{\text{L}}K_{\text{R}}| \otimes \langle\text{PC},\sigma_-|$$
$$- B^*|K'_{\text{ex,L}}K_{\text{L}}K'_{\text{R}}\rangle\langle K_{\text{L}}K'_{\text{R}}| \otimes \langle\text{PC},\sigma_+| - A^*|K'_{\text{ex,L}}K_{\text{L}}K'_{\text{R}}\rangle\langle K_{\text{L}}K'_{\text{R}}| \otimes \langle\text{PC},\sigma_-| + \text{h.c.},$$

$$H_{\text{PC-output}} = \sum_{\substack{\sigma=\sigma_+,\sigma_-;\\ \tau=K,K';\\ \vec{k}_{2\text{D}}}} (T_k|\tau'_{\text{L}}\tau_{\text{R}}\rangle \otimes |\overrightarrow{k}_{2\text{D}},\sigma\rangle\langle\tau'_{\text{L}}\tau_{\text{R}}| \otimes \langle\text{PC},\sigma| + \text{h.c.}),$$

$$H_{SE} = \sum_{\sigma=\sigma_+,\sigma_-;\tau=K,K';\mu} (\gamma_\mu|\tau'_{\text{L}}\tau_{\text{R}}\rangle|\mu,\sigma\rangle\langle\tau_{\text{ex,L}}\tau'_{\text{L}}\tau_{\text{R}}| + \text{h.c.}). \tag{12}$$

The above Hamiltonian includes contributions from several subsystems. H_{input} comes from the photon states that are outside the DBR cavity and propagate along the cavity axis, with $k_{1\text{D}}$ the wave vector of the photon; H_{DC} comes from the DBR cavity modes with ω_{DC} as the mode frequency; H_{trion} comes from the trion states with ω_{trion} as the trion frequency

(relative to that of the qubit electron in QD_L); H_{PC} comes from the PC cavity modes with ω_{PC} as the mode frequency; H_{output} comes from the photon states that are outside the PC cavity and propagate in the plane, with k_{2D} being the wave vector of the photon; and $H_{reservoir}$ comes from the photon reservoir, excluding the contributions H_{input}, H_{DC}, H_{PC}, and H_{output} (μ = photonstatelabel and ω_μ = photonfrequency). Throughout the paper, we assume the resonance condition $\omega_{ph} = \omega_{DC} = \omega_{PC} = \omega_{trion}$. The Hamiltonian also includes couplings among the subsystems $H_{input\text{-}DC}$ describes the tunneling of photons into and out of the DBR cavity with h.c. stands for the hermitian conjugate; $H_{DC\text{-}trion}$ describes the coupling between the DBR cavity mode and the trion; $H_{trion\text{-}PC}$ describes the coupling between the trion and the PC cavity mode; $H_{PC\text{-}output}$ describes the tunneling of photons into and out of the PC cavity; and H_{SE} describes the coupling between the trion and the photon reservoir with the coupling constant γ_μ. Several approximations have been made above or will be made below. For example, we take $\kappa_k \approx \sqrt{c\kappa_{DC}/L}$ ($T_k \approx \sqrt{2c^2\Gamma_{PC}/L^2\omega_{PC}}$) independent of the wave number under the flat-band assumption, with $2\kappa_{DC}(2\Gamma_{PC}) =$ leakage rate of the DBR cavity (PC cavity) mode. Equivalently, this means that we ignore the leakage into the reservoir and take the leakage rate to be primarily due to the coupling $H_{input\text{-}DC}$ ($H_{PC\text{-}output}$), with $\kappa_{DC} \approx \pi\sum_{k_{1D}} |\kappa_k|^2\delta(\omega_{DC} - c|k_{1D}|)$ ($\Gamma_{PC} \approx \pi\sum_{\vec{k}_{2D}} |T_k|^2\delta(\omega_{PC} - c|\vec{k}_{2D}|)$). Moreover, in Eq. (12) we have neglected the exchange process $|K_{ex,L}, K'_L\rangle \leftrightarrow |K'_{ex,L}, K_L\rangle$ where the simultaneous valley flips of three carriers are involved. As such a process is of high order, it is neglected in the equation. This approximation decouples the amplitudes of the trion states $|K_{ex,L}, K'_L\rangle$ and $|K'_{ex,L}, K_L\rangle$ and, thus, facilitates the solution to the wave equation, as will become clear below. Last, the rate of trion emission into the reservoir is given by $2\gamma_{SE}(\omega) = 2\pi\sum_\mu |\gamma_\mu|^2\delta(\omega - \omega_\mu)$. We take $\gamma_{SE}(\omega)$ as a phenomenological constant that also accounts for nonradiative decay of the trion.

B. Wave equation and solution

Using the Hamiltonian specified above, we set up the wave equation for the system. For typical applications, as the cavity leakage rates Γ_{PC} and κ_{DC} scale inversely with the corresponding cavity Q factors, we take them to be the maximum frequency parameters so as not to impose stringent requirements on the Q factors. Moreover, we take $|B/A| \ll 1$, according to the numerical estimate obtained in Sec. II C for a typical QD.

The wave equation consists of coupled differential equations for the 14 amplitudes $\{\phi^{DC}_{\sigma\tau}, \phi^{trion}_{\tau}, \phi^{PC}_{\sigma\tau}, \phi^{output}_{\sigma\tau}\}$, which are divided into three sets and approximately solved. The three sets of equations describe the key subprocesses in the QST, respectively, as follows.

The first set of equations govern $\phi^{DC}_{\sigma\tau}$ and the process incident signal photon → DBR cavity photon. They are given by

$$i\partial_t\phi^{DC}_{\sigma\tau}(t) \approx (\omega_{DC} - i\kappa_{DC})\phi^{DC}_{\sigma\tau}(t) + \sqrt{2c\kappa_{DC}/L}\,\phi^{input}_{\sigma\tau}(t) \tag{13}$$

Equation (13) takes $\phi^{DC}_{\sigma\tau}$ to be primarily determined by the incoming signal $\phi^{input}_{\sigma\tau}$ and the damping (κ_{DC}) of DBR cavity modes. For simplification, it neglects the contributions from the process of photon emission by the trion or that of photon absorption by the qubit, both of which occur only after the entry of signal photon into the cavity, as indicated in Fig. 4, and hence are higher order processes from the perturbation-theoretical point of view. After solving Eq. (13), $\phi^{DC}_{\sigma\tau}$ is given in terms of the input by

$$\phi^{DC}_{\sigma\tau}(t) = i\bar{\alpha}(\sigma,\tau)\sqrt{c\kappa_{DC}/L}\int_0^t dt' e^{-i(\omega_{DC}-i\kappa_{DC})(t-t')}G(t'), \tag{14}$$

$$\bar{\alpha}(\sigma_+,K) = \alpha, \bar{\alpha}(\sigma_+,K') = -\alpha,$$
$$\bar{\alpha}(\sigma_+,K') = \beta, \bar{\alpha}(\sigma_-,K') = -\beta$$

The second set of equations governs ϕ^{trion}_{τ}, $\phi^{PC}_{\sigma\tau}$, and the resonant process of photon + electron ↔ trion. For the specific process $|\text{photon}, K_L\rangle \leftrightarrow |K'_{ex}, K_L\rangle$, for example, we obtain

$$i\partial_t\begin{pmatrix}\phi^{tri}_K(t)\\ \phi^{PC}_{\sigma_+K}(t)\\ \phi^{PC}_{\sigma_-K}(t)\end{pmatrix} = \begin{pmatrix}(\omega_{trion} - i\gamma_{total}) & A & B\\ A^* & (\omega_{PC} - i\Gamma_{PC}) & 0\\ B^* & 0 & (\omega_{PC} - i\Gamma_{PC})\end{pmatrix} \times \begin{pmatrix}\phi^{tri}_K(t)\\ \phi^{PC}_{\sigma_+K}(t)\\ \phi^{PC}_{\sigma_-K}(t)\end{pmatrix} + \begin{pmatrix}C\phi^{DC}_{\sigma_+K}(t) + D\phi^{DC}_{\sigma_-K}(t)\\ 0\\ 0\end{pmatrix}$$
$$\gamma_{total} = \gamma_{SE} + \gamma_{tD}. \tag{15}$$

γ_{SE}, γ_{tD}, and Γ_{PC} account for trion and PC cavity photon decays due to the couplings H_{SE}, $H_{DC\text{-}trion}$, and $H_{PC\text{-}output}$, respectively. $\gamma_{tD} \approx \pi|C|^2D_{os} = |C|^2/\kappa_{DC}$, where $D_{os} = 1/\pi\kappa_{DC}$ is the density of states for the DBR cavity mode with level broadening due to the cavity leakage. Note that the DBR cavity photon, with the amplitude $\phi^{DC}_{\sigma\tau}$ determined by Eq. (14), now provides a source term to Eq. (15), feeding photons into the resonant process. For the other process $|\text{photon}, K'_L\rangle \leftrightarrow |K_{ex}, K'_L\rangle$, a similar set of equations are obtained by an appropriate change of valley and polarization subscripts in Eq. (15).

Last, the third set of equations governs $\phi^{output}_{\sigma\tau}$ and describes the process PC cavity photon → outgoing photon:

$$i\partial_t\phi^{output}_{\sigma\tau}(k_{2D},t) = T_k\phi^{PC}_{\sigma\tau}(t) + \omega_{output}\phi^{output}_{\sigma\tau}(t), \tag{16}$$

where $\omega_{output} = c|\vec{k}_{2D}|$. The argument k_{2D} in $\phi^{output}_{\sigma\tau}$ will be omitted below when it does not cause confusion.

In order to solve Eqs. (15) and (16), we perform a linear transformation and obtain

$$i\partial_t \begin{pmatrix} \phi_K^{\text{trion}}(t) \\ \phi_{K1}^{\text{PC}}(t) \\ \phi_{K2}^{\text{PC}}(t) \end{pmatrix} = \begin{pmatrix} (\omega_{\text{trion}} - i\gamma_{\text{total}}) & \sqrt{|A|^2+|B|^2} & 0 \\ \sqrt{|A|^2+|B|^2} & (\omega_{\text{PC}} - i\Gamma_{\text{PC}}) & 0 \\ 0 & 0 & (\omega_{\text{PC}} - i\Gamma_{\text{PC}}) \end{pmatrix} \begin{pmatrix} \phi_K^{\text{trion}}(t) \\ \phi_{K1}^{\text{PC}}(t) \\ \phi_{K2}^{\text{PC}}(t) \end{pmatrix} + \begin{pmatrix} C\phi_{\sigma_+ \text{K}}^{\text{DC}}(t) + D\phi_{\sigma_- K}^{\text{DC}}(t) \\ 0 \\ 0 \end{pmatrix} \tag{17}$$

and

$$i\partial_t \begin{pmatrix} \phi_{K1}^{\text{output}}(t) \\ \phi_{K2}^{\text{output}}(t) \end{pmatrix} = T_k \begin{pmatrix} \phi_{K1}^{\text{PC}}(t) \\ \phi_{K2}^{\text{PC}}(t) \end{pmatrix} + \omega_{\text{output}} \begin{pmatrix} \phi_{K1}^{\text{output}}(t) \\ \phi_{K2}^{\text{output}}(t) \end{pmatrix} \tag{18}$$

with the transformation given by

$$\begin{aligned} \phi_{K1}^{\text{PC}}(t) &= \frac{A}{\sqrt{|A|^2+|B|^2}}\phi_{\sigma_+ K}^{\text{PC}}(t) + \frac{B}{\sqrt{|A|^2+|B|^2}}\phi_{\sigma_- K}^{\text{PC}}(t) \\ \phi_{K2}^{\text{PC}}(t) &= -\frac{B^*}{\sqrt{|A|^2+|B|^2}}\phi_{\sigma_+ K}^{\text{PC}}(t) + \frac{A^*}{\sqrt{|A|^2+|B|^2}}\phi_{\sigma_- K}^{\text{PC}}(t) \end{aligned} \tag{19}$$

and

$$\begin{aligned} \phi_{K1}^{\text{output}}(t) &= \frac{A}{\sqrt{|A|^2+|B|^2}}\phi_{\sigma_+ K}^{\text{output}}(t) + \frac{B}{\sqrt{|A|^2+|B|^2}}\phi_{\sigma_- K}^{\text{output}}(t) \\ \phi_{K2}^{\text{output}}(t) &= -\frac{B^*}{\sqrt{|A|^2+|B|^2}}\phi_{\sigma_+ K}^{\text{output}}(t) + \frac{A^*}{\sqrt{|A|^2+|B|^2}}\phi_{\sigma_- K}^{\text{output}}(t). \end{aligned} \tag{20}$$

The transformed equations can be solved as follows. First, the block of top two rows in Eq. (17) forms a two-component time-dependent Schrodinger equation with a source term,

$$i\partial_t \begin{pmatrix} \phi_K^{\text{trion}}(t) \\ \phi_{K1}^{\text{PC}}(t) \end{pmatrix} = H_0 \begin{pmatrix} \phi_K^{\text{trion}}(t) \\ \phi_{K1}^{\text{PC}}(t) \end{pmatrix} + |f(t)\rangle, \tag{21}$$

where

$$H_0 = \begin{pmatrix} a & \sqrt{|A|^2+|B|^2} \\ \sqrt{|A|^2+|B|^2} & b \end{pmatrix}, \quad a \equiv \omega_{\text{trion}} - i\gamma_{\text{total}}, b \equiv \omega_{\text{PC}} - i\Gamma_{\text{PC}}, \quad |f(t)\rangle \equiv \begin{pmatrix} C\phi_{\sigma_+ K}^{\text{DC}}(t) + D\phi_{\sigma_- K}^{\text{DC}}(t) \\ 0 \end{pmatrix}. \tag{22}$$

The solution to Eq. (21) with the initial condition $\phi_K^{\text{trion}}(0) = \phi_{K1}^{\text{PC}}(0) = 0$ is given by

$$\begin{pmatrix} \phi_K^{\text{trion}}(t) \\ \phi_{K1}^{\text{PC}}(t) \end{pmatrix} = -i \sum_{n=1,2} |\varphi_n\rangle \int_0^t e^{-i\lambda_n(t-t')}(\varphi_n|f(t'))dt', \tag{23}$$

where $|\varphi_n\rangle$ and λ_n for $n = 1,2$ are, respectively, the eigenvectors and eigenvalues of H_0 given in the Appendix. Using the expressions there, one can show that $\lambda_1 \approx \omega_{\text{ph}} + O(\Gamma_{\text{PC}})$ and $\lambda_2 \approx \omega_{\text{ph}} + O(\max(\gamma_{\text{total}}, \gamma_{tp}))$ under the resonance condition, with $\gamma_{tp} \equiv |A|^2/\Gamma_{\text{PC}}$ the rate of photon emission by the trion into the PC cavity mode. $(\varphi_n|f(t'))$ in Eq. (23) denotes the projection of $|f(t')\rangle$ onto $|\varphi_n\rangle$ in the case where H_0 is non-Hermitian (see the Appendix). Last, the third row of Eq. (17) can easily be solved. With initial condition $\phi_{K2}^{\text{PC}}(0) = 0$, it leads to $\phi_{K2}^{\text{PC}}(t) = 0$.

In the output from the system, Eq. (18) gives the outgoing photon amplitude

$$\phi_{K1}^{\text{output}}(t) = -iT_k \int_0^t \phi_{K1}^{\text{PC}}(t')e^{-i\omega_{\text{output}}(t-t')}dt' \tag{24}$$

and a similar expression for $\phi_{K2}^{\text{output}}(t)$. By substituting $\phi_{K1}^{\text{PC}}(t)$ and $\phi_{K2}^{\text{PC}}(t)$ obtained above, we find that the amplitudes at the completion of QST, with the corresponding probabilities given by (see the Appendix),

$$\lim_{x_0 \to -\infty} \left|\phi_{K1}^{\text{output}}(k_{2\text{D}}, t \to \infty)\right|^2 = 2\sqrt{\pi}\frac{\kappa_{\text{DC}}}{\Delta\omega_{\text{ph}}} e^{-(\omega_{\text{output}}(k_{2\text{D}})-\omega_{\text{ph}})^2/\Delta\omega_{\text{ph}}^2} \frac{|T_k|^2|\alpha C + \beta D|^2(|A|^2+|B|^2)}{|(\omega_{\text{output}}(k_{2\text{D}})-\lambda_1)(\omega_{\text{output}}(k_{2\text{D}})-\lambda_2)(\omega_{\text{output}}(k_{2\text{D}})-\lambda_3)|^2},$$

$$\left|\phi_{K2}^{\text{output}}(k_{2\text{D}}, t \to \infty)\right|^2 = 0, \lambda_3 \equiv \omega_{\text{DC}} - i\kappa_{\text{DC}}. \tag{25}$$

A similar procedure obtains $|\phi^{\text{output}}_{K'1}(k_{2D},\infty)|^2$ and $|\phi^{\text{output}}_{K'2}(k_{2D},\infty)|^2$, with $|\alpha C+\beta D|^2$ in $|\phi^{\text{output}}_{K1}(k_{2D},\infty)|^2$ replaced by $|\alpha D^*+\beta C^*|^2$, and $|\phi^{\text{output}}_{K'2}(k_{2D},\infty)|^2=0$.

For the yield, using the foregoing solutions, we derive the figure of merits for the photon-valley QST. First, the yield is given by integrating the various output amplitudes as follows:

$$P=\sum_{\sigma,\tau,k_{2D}}\left|\phi^{\text{output}}_{\sigma\tau}(k_{2D},\infty)\right|^2=\sum_{k_{2D}}P_{k_{2D}},$$

$$P_{k_{2D}}\equiv\left|\phi^{\text{output}}_{K1}(k_{2D},\infty)\right|^2+\left|\phi^{\text{output}}_{K'1}(k_{2D},\infty)\right|^2, \quad (26)$$

with $P_{k_{2D}}$ as the yield for a given k_{2D}. This gives

$$P=\frac{2}{\sqrt{\pi}}\frac{\kappa_{DC}\Gamma_{PC}}{\Delta\omega_{ph}}[|\alpha C+\beta D|^2+|\alpha D^*+\beta C|^2]\times(|A|^2+|B|^2)I_w,$$

$$I_w\equiv\int d\omega_{\text{output}}\frac{e^{-(\omega_{\text{output}}-\omega_{ph})^2/\Delta\omega_{ph}^2}}{|(\omega_{\text{output}}-\lambda_1)(\omega_{\text{output}}-\lambda_2)(\omega_{\text{output}}-\lambda_3)|^2}. \quad (27)$$

In order to gain insights into the dependence of P on various parameters, we analyze the frequency integral I_w in the following. In essence, it is primarily determined by various frequency parameters, such as the photon bandwidth $\Delta\omega_{ph}$ of the Gaussian function $e^{-(\omega_{\text{output}}(k_{2D})-\omega_{ph})^2/\Delta\omega_{ph}^2}$ and the poles λ_1, λ_2, and λ_3 in the integrand. In accordance with the condition given earlier that Γ_{PC} and κ_{DC} are taken to be the maximum frequency parameters, we consider the two following cases, namely, Case 1 where $\min(\Gamma_{PC},\kappa_{DC})\geqslant\max(\gamma_{\text{total}},\gamma_{tP})\geqslant\Delta\omega_{ph}$ and Case 2 where $\min(\Gamma_{PC},\kappa_{DC})\geqslant\Delta\omega_{ph}\geqslant\max(\gamma_{\text{total}},\gamma_{tP})$. Below we express P in terms of the dimensionless frequencies $\gamma'_{tD}\equiv\gamma_{tD}/\gamma_{tP}$, $\gamma'_{SE}\equiv\gamma_{SE}/\gamma_{tP}$, and $\Delta\omega'_{ph}\equiv\Delta\omega_{ph}/\gamma_{tP}$, in the two cases.

Case 1. For $\min(\Gamma_{PC},\kappa_{DC})\geqslant\max(\gamma_{\text{total}},\gamma_{tP})\geqslant\Delta\omega_{ph}$,

$$P\approx\frac{2}{\sqrt{\pi}}\eta_1\frac{\gamma'_{tD}}{\max((\gamma'_{tD}+\gamma'_{SE})^2,1)}. \quad (28)$$

η_1 is a dimensionless, order of unity coefficient with weak dependence on all frequencies, given by

$$\eta_1\equiv\frac{\Gamma_{PC}{}^2\max(\gamma_{\text{total}}{}^2,\gamma_{tP}{}^2)\kappa_{DC}{}^2}{\Delta\omega_{ph}}I_w\times(\Delta\omega_{ph},\kappa_{DC},\gamma_{\text{total}},\gamma_{tP},\Gamma_{PC}), \quad (29)$$

which also indicates how I_w scales with the various frequencies.

Case 2. For $\min(\Gamma_{PC},\kappa_{DC})\geqslant\Delta\omega_{ph}\geqslant\max(\gamma_{\text{total}},\gamma_{tP})$,

$$P\approx\frac{2}{\sqrt{\pi}}\eta_2\frac{\gamma'_{tD}}{\max(\gamma'_{tD}+\gamma'_{SE},1)}\frac{1}{\Delta\omega'_{ph}}. \quad (30)$$

The dimensionless coefficient η_2 is also of the order of unity and given by

$$\eta_2\equiv\Gamma_{PC}{}^2\max(\gamma_{\text{total}},\gamma_{tP})\kappa_{DC}{}^2I_w(\Delta\omega_{ph},\kappa_{DC},\gamma_{\text{total}},\gamma_{tP},\Gamma_{PC}). \quad (31)$$

For the optimal condition for yield, the above result suggests to optimize P with the following choice of parameters: $\gamma'_{tD}\sim 1>\gamma'_{SE}$(i.e., $\gamma_{tD}\sim\gamma_{tP}>\gamma_{SE}$), along with $\min(\Gamma_{PC},\kappa_{DC})\geqslant\gamma_{tP}\geqslant\Delta\omega_{ph}$ (i.e., the condition given in Case 1). The condition $\gamma_{tD}\approx\gamma_{tP}$ (or $|A|^2/\Gamma_{PC}\approx|C|^2/\kappa_{DC}$) means the trion emits a photon into the DBR and PC cavity modes with nearly matching rates, at least in order of magnitudes, which imposes a constraint of correlation between the two cavities' parameters. In Sec. IV, a numerical evaluation of the integral I_w will be performed for a more detailed study of P as a function of the various parameters.

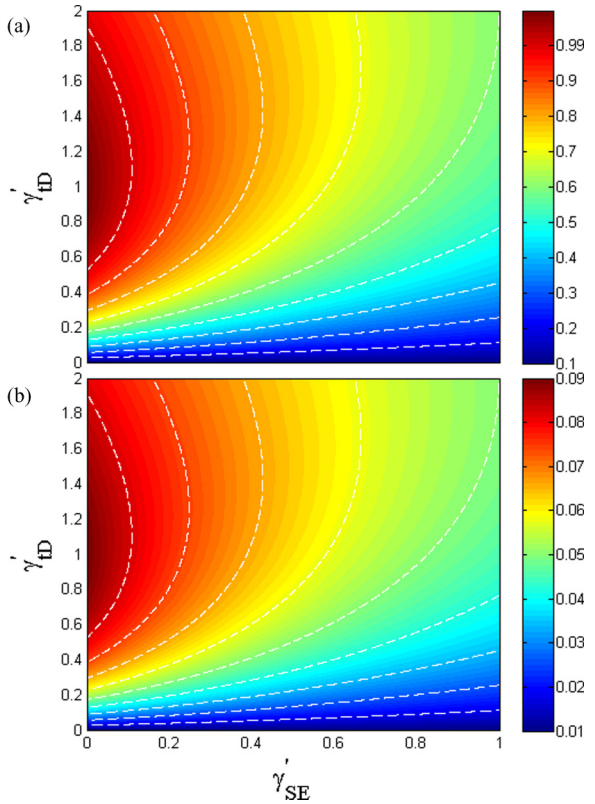

FIG. 5. Contour plots of the yield P as a function of trion decay rates γ'_{SE} (nonradiative damping and radiative damping into noncavity modes) and γ'_{tD} (radiative damping into DBR cavity modes), with different photon band widths: $\Delta\omega'_{ph}=0.5$ in (a) and $\Delta\omega'_{ph}=5$ in (b).

Next, the fidelity of QST is defined by $F(\alpha,\beta)=\langle\Psi_{\text{ideal}}|\hat{\rho}_{\text{output}}|\Psi_{\text{ideal}}\rangle/P$, where Ψ_{ideal} is given by Eq. (6) and $\hat{\rho}_{\text{output}}=\sum_{\sigma\tau,\sigma'\tau';k_{2D}}\phi^{\text{output}}_{\sigma\tau}(k_{2D},\infty)\phi^{\text{output}}_{\sigma'\tau'}(k_{2D},\infty)^*$ is the density matrix of the final state. Alternatively, we write

$$F(\alpha,\beta)=\sum_{k_{2D}}F_{k_{2D}}P_{k_{2D}}/P,$$

$$F_{k_{2D}}\equiv\langle\Psi_{\text{ideal}}|\sum_{\sigma\tau,\sigma'\tau'}\phi^{\text{output}}_{\sigma\tau}(k_{2D},\infty)\phi^{\text{output}}_{\sigma'\tau'}(k_{2D},\infty)^*\times|\Psi_{\text{ideal}}\rangle/P_{k_{2D}}, \quad (32)$$

with $F_{k_{2D}}$ as the fidelity for a given k_{2D}. Using the output amplitudes obtained earlier, one can show that $F_{k_{2D}}$ is a constant independent of k_{2D} and thus obtain

$$F(\alpha,\beta)=F_{k_{2D}} \quad (33)$$

$$=\frac{|\alpha^*A^*(\alpha C+\beta D)+\beta^*A(\alpha D^*+\beta C^*)|^2}{[|(\alpha C+\beta D)|^2+|(\alpha D^*+\beta C^*)|^2][|A|^2+|B|^2]}$$

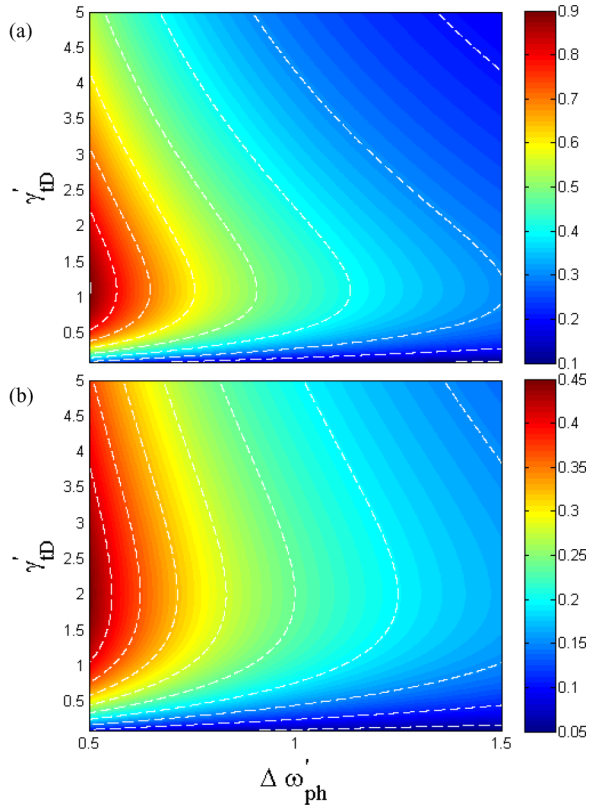

FIG. 6. Contour plots of the yield P as a function of $\Delta\omega'_{\rm ph}$ (photon band width) and γ'_{tD} (radiative trion damping into DBR cavity modes). The effect of trion decay rate γ'_{SE} (nonradiative damping and radiative damping into noncavity modes) on yield is studied with (a) $\gamma'_{SE} = 0.1$ and (b) $\gamma'_{SE} = 1$.

We note that F given above is a function of the incoming photon state (α,β). One could further take the average of F with respect to (α,β). Instead, in what follows, we will present the numerical results for both P and F, with F being given for representative (α,β)s, e.g., $(1,0)$, $(1/\sqrt{2}, 1/\sqrt{2})$, etc. The issue of optimization as well as that of minimizing the sensitivity to (α,β) will be discussed in Sec. IV when we present the numerical result.

IV. NUMERICAL STUDY

We present numerical results of the yield and fidelity. Effects of damping parameters γ_{SE}, $\kappa_{\rm DC}$, and $\Gamma_{\rm PC}$, photon bandwidth Δw_{ph}, and magnitudes of major optical matrix elements A and C will be discussed. For the fidelity F, we will examine effects of the ratio $B/A(= D/C)$ between major and minor optical matrix elements, since F depends critically on it.

We start with an estimation of P and F in a typical case. We use $\omega_{\rm ph}$ and the corresponding numerical values of optical matrix elements given in Sec. II, namely, $\omega_{\rm ph} = 1.6 \cdot 10^5$ GHz, $B/A = D/C \sim 0.04$, $A \sim 45$ GHz, and $C \sim 30$ GHz, with all the matrix elements here taken to be real numbers. Moreover, we take $\gamma_{SE} = 1$ GHz, $\Delta\omega_{\rm ph} = 5$ GHz, $\kappa_{\rm DC} = \omega_{\rm ph}/\pi Q = 90$ GHz corresponding to a cavity $Q \sim 550$, $\Gamma_{\rm PC} = 200$ GHz corresponding to $Q \sim 250$, and $(\alpha,\beta) = (1,0)$. The numerical

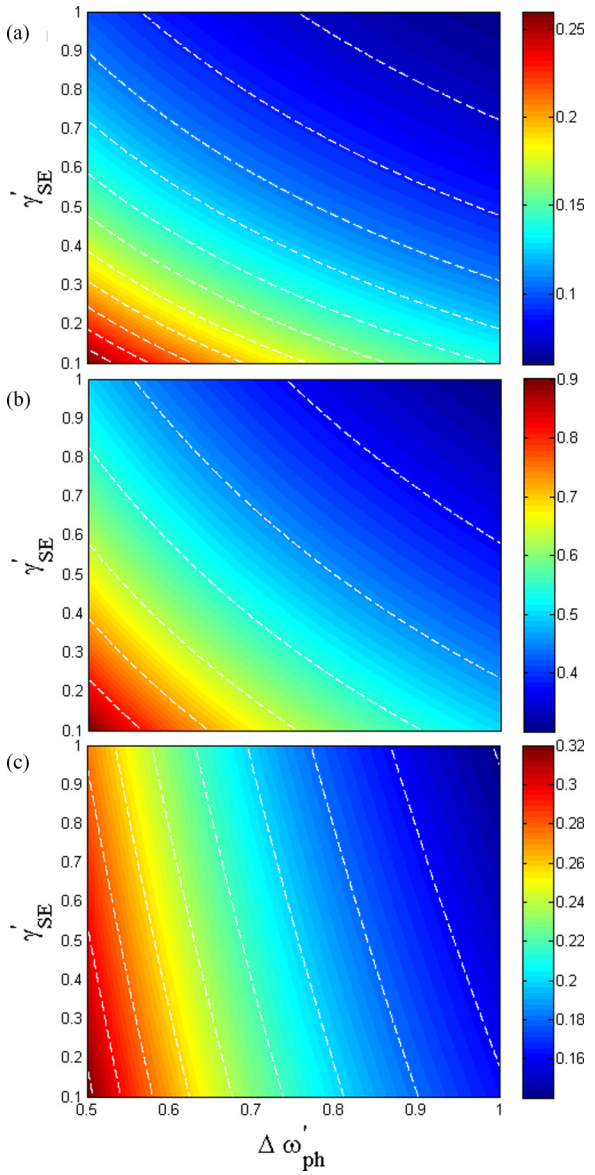

FIG. 7. Contour plots of the yield P as a function of the trion decay rate γ'_{SE} (nonradiative damping as well as damping into noncavity modes) and $\Delta\omega'_{ph}$ (photon band width), for different γ'_{tD} (trion damping into DBR cavity modes), with (a) $\gamma'_{tD} = 0.1$, (b) $\gamma'_{tD} = 1$, and (c) $\gamma'_{tD} = 10$.

estimation of P and F using the above parameters in Eqs. (27) and (33) gives $P \sim 0.998$ and $F \sim 0.998$.

Next, we discuss the yield P as a function of γ'_{tD} (radiative trion damping into DBR cavity modes), γ'_{SE} (nonradiative trion damping and radiative trion damping into noncavity modes), and $\Delta\omega'_{\rm ph}$ (photon band width), under the condition given in Sec. III for Cases 1 and 2, namely, that $\Gamma_{\rm PC}$ and $\kappa_{\rm DC}$ are the largest frequency parameters.

Figure 5 presents the yield P as a function of the two trion damping rates, γ'_{SE} and γ'_{tD}, for different $\Delta\omega'_{\rm ph}$, with $\Delta\omega'_{\rm ph} = 0.5$ in Fig. 5(a) and $\Delta\omega'_{\rm ph} = 5$ in Fig. 5(b). Generally, we see that P decreases with increasing γ'_{SE}. On the other hand, P varies nonmonotonously with γ'_{tD}, in such a way that in Fig. 5(a), P attains the maximum $\sim$1 around $\gamma'_{tD} \sim 1$

for small γ'_{SE}. In contrast, in Fig. 5(b), with $\Delta\omega'_{\rm ph} = 5$, it violates the condition specified for Case 1 and hence also the optimal condition for P. Therefore, P is typically small in this case.

Figure 6 presents the yield P as a function of γ'_{tD} and $\Delta\omega'_{\rm ph}$. The effect of γ'_{SE} on yield is studied with $\gamma'_{SE}= 0.1$ in Fig. 6(a) and $\gamma'_{SE}= 1$ in Fig. 6(b). We see that generally P decreases with increasing $\Delta\omega'_{\rm ph}$ but varies nonmonotonously with γ'_{tD}, with the maximum value $\sim$1 reached at small $\Delta\omega'_{\rm ph}$ in Fig. 6(a). In Fig. 6(b), because of the relatively large magnitude of γ'_{SE}, P is overall reduced in comparison to that in Fig. 6(a).

Figure 7 presents the yield P as a function of γ'_{SE} and $\Delta\omega'_{\rm ph}$, for different γ'_{tD}s, with (a) $\gamma'_{tD} = 0.1$, (b) $\gamma'_{tD} = 1$, and (c)$\gamma'_{tD} = 10$. We see that P generally decreases with both increasing γ'_{SE} and $\Delta\omega'_{\rm ph}$. Moreover, it varies nonmonotonously with γ'_{tD}, with its value in Figs 7(a) and 7(c) being overall reduced in comparison to that in Fig. 7(b), where $\gamma'_{tD} = 1$.

The results shown in Figs. 5–7 indicate that minimizing the trion damping rate γ'_{SE} is generally beneficial to the QST yield. In addition, a narrow $\Delta\omega'_{\rm ph}$ that favors the QST to proceed near the resonance condition enhances the yield. Overall, we see that the yield reaches the maximum $\sim$1 when $\gamma'_{tD} \sim 1$, $\Delta\omega'_{\rm ph} < 1$, and $\gamma'_{SE} < 1$, confirming the optimal condition given in Sec. III B.

Next, we discuss the fidelity F as a function of A, B, C, D, α, and β. In particular, we will examine effects of the ratios $|B/A|$ and $|\beta/\alpha|$, the phase of D/C (denoted as $\phi_{D/C}$), and the phase of β/α (denoted as $\phi_{\beta/\alpha}$). We take A and C to be real throughout the discussion.

Figure 8 presents the fidelity F as a function of $|B/A|$ and $\phi_{D/C}$, with (a) $\alpha = 1$, $\beta = 0$, (b) $\alpha = 1/\sqrt{2}$, $\beta = 1/\sqrt{2}$, and (c) $\alpha = 1/\sqrt{2}$, $\beta = i/\sqrt{2}$. Overall, we see that F decreases with increasing $|B/A|$. On the other hand, while F is independent of $\phi_{D/C}$ in the case of Fig. 8(a), where the incoming photon signal consists of single circular polarization, in Figs. 8(b) and 8(c) F varies periodically in $\phi_{D/C}$, with a relative phase shift by $\pi/2$ between the two figures. These features can be understood in terms of the fidelity formula given in Eq. (33). By substituting $B = A|B/A|e^{i\phi_{D/C}}$ and $\beta = \alpha|\beta/\alpha|e^{i\phi_{\beta/\alpha}}$ into the formula, we obtain, in the case of $|\alpha| = |\beta| = 1/\sqrt{2}$,

$$F = \frac{|C + |D|\cos\delta|^2}{|C|^2 + |D|^2 + 2C|D|\cos\delta}\,\frac{|A|^2}{|A|^2 + |B|^2}, \tag{34}$$

where δ=$\phi_{D/C} + \phi_{\beta/\alpha}$, which shows that F is indeed periodic in $\phi_{D/C}$, and is shifted in $\phi_{D/C}$ in the presence of a finite $\phi_{\beta/\alpha}$. Moreover, the local maximum and minimum occur at $\delta = n\pi$ and $\delta = (n + 1/2)\pi$, respectively, where n = integer. However, although the fidelity varies with $\phi_{\beta/\alpha}$, its overall sensitivity to the incoming signal state can be suppressed by reducing $|B/A|$, as reflected in both Eq. (34) and Fig. 8.

Last, Fig. 9 presents the dependence of fidelity F on both $|\beta/\alpha|$ and $\phi_{\beta/\alpha}$, for different combinations of $|B/A|$ and $\phi_{D/C}$, with (a) $|B/A| = 0.04$, $\phi_{D/C} = 0$; (b) $|B/A| = 0.04$, $\phi_{D/C} = \pi/4$; (c) $|B/A| = 0.04$, $\phi_{D/C} = \pi/2$; (d) $|B/A| = 0.4$, $\phi_{D/C} = 0$; (e) $|B/A| = 0.4$, $\phi_{D/C} = \pi/4$; and (f) $|B/A| = 0.4$, $\phi_{D/C} = \pi/2$. We see that F in Figs. 9(a)–9(c) with $|B/A| = 0.04$ is generally larger than that in Figs. 9(d)–9(f), with $|B/A| = 0.4$. Moreover, with $|B/A|$ being small in Figs. 9(a)–9(c), $F \sim 1$ and is quite robust to the variations in both $|\beta/\alpha|$ and $\phi_{\beta/\alpha}$. In detail, F increases with $|\beta/\alpha|$ and reaches the maximum at $|\beta/\alpha| = 1$. Beyond that, although not shown in the graphs, F would be expected to decrease from the maximum when further increasing $|\beta/\alpha|$, since, as Eq. (33) indicates, F is basically a symmetric function of α and β. On the other hand, F varies periodically with $\phi_{\beta/\alpha}$ and is shifted by $\phi_{D/C} = \pi/4$ when going from Figs. 9(a) to 9(b) or from Figs. 9(d) to 9(e) and is shifted by $\phi_{D/C} = \pi/2$ when going from Figs. 9(a) to 9(c) or from Figs. 9(d) to 9(f), with the local maximum and minimum occurring at $\phi_{D/C} + \phi_{\beta/\alpha} = n\pi$ and $\phi_{D/C} + \phi_{\beta/\alpha} = (n + 1/2)\pi$, respectively, where n = integer. The periodic behavior displayed here can again be understood in terms of an analysis similar to the earlier one performed for Fig. 8.

In the optimal condition for fidelity, overall, Figs. 8 and 9 show that the fidelity F depends on $|\beta/\alpha|$ and $\phi_{\beta/\alpha}$ of the incoming signal and $|B/A|$ and $\phi_{D/C}$ of the valley-pair qubit. From the application point of view, they also make the following important suggestion, namely, reduction of the

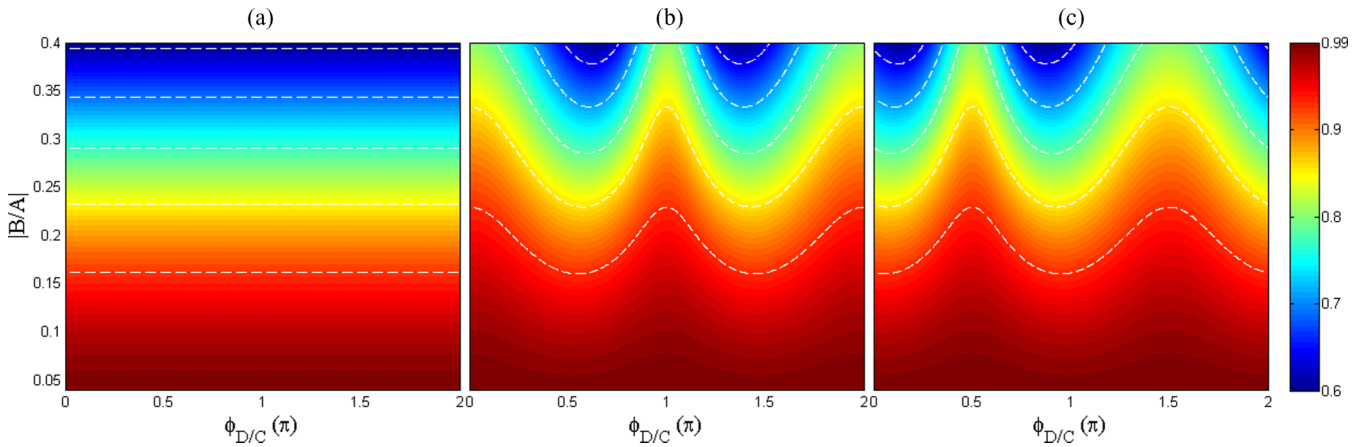

FIG. 8. Contour plots of the fidelity F as a function of $|B/A|$ and the relative phase $\phi_{D/C}$ for different combinations of α and $\beta = 0$: (a) $\alpha = 1$, $\beta = 0$; (b) $\alpha = 1/\sqrt{2}$, $\beta = 1/\sqrt{2}$; and (c) $\alpha = 1/\sqrt{2}$, $\beta = i/\sqrt{2}$.

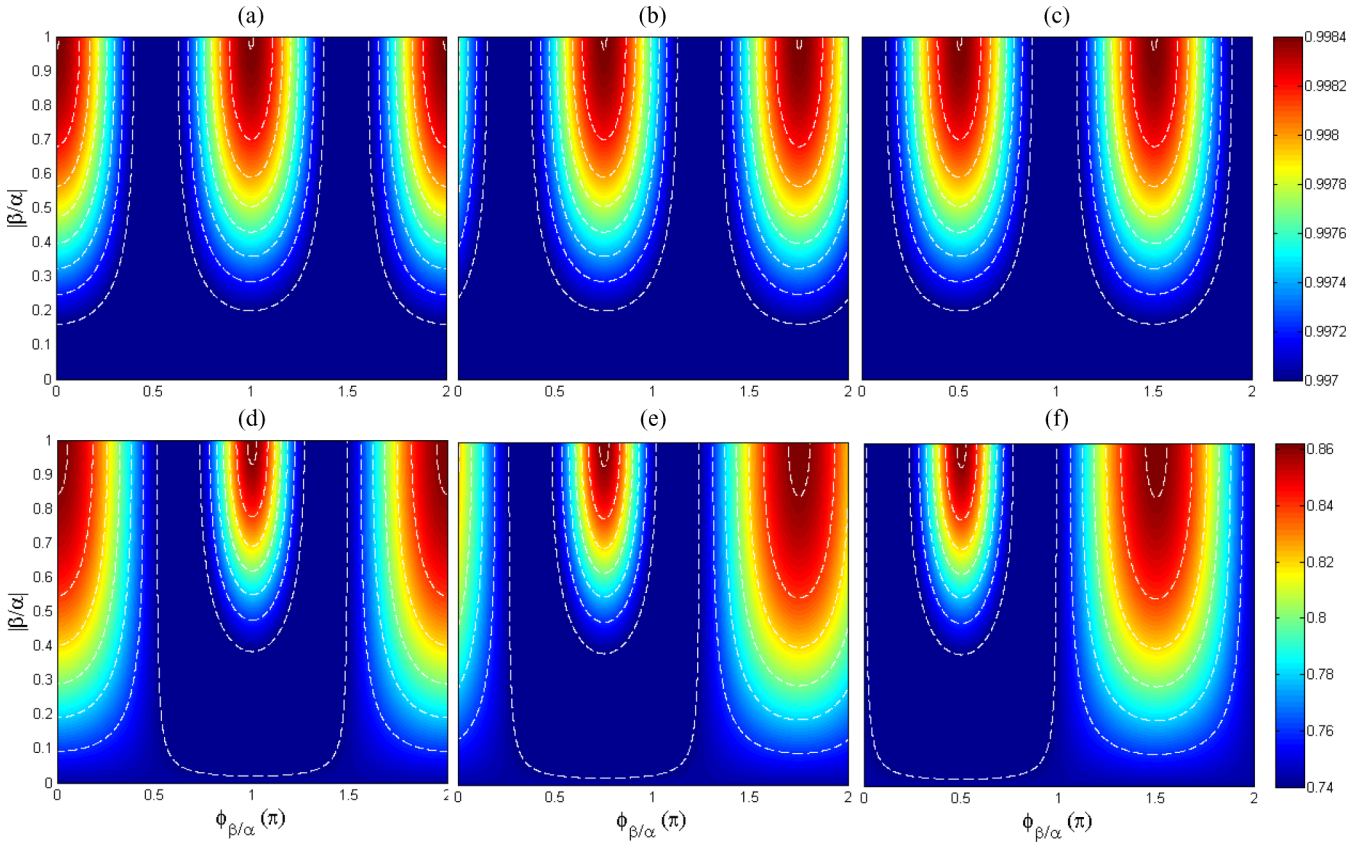

FIG. 9. Contour plot of fidelity as a function of the photon amplitude ratio $|\beta/\alpha|$ and relative phase $\phi_{\beta/\alpha}$. The effect of $|B/A|$ and $\phi_{\beta/\alpha}$ on fidelity is investigated separately, each under different combinations, namely, (a) $|B/A| = 0.04$, $\phi_{D/C} = 0$; (b) $|B/A| = 0.04$, $\phi_{D/C} = \pi/4$, (c) $|B/A| = 0.04$, $\phi_{D/C} = \pi/2$; (d) $|B/A| = 0.4$, $\phi_{D/C} = 0$; (e) $|B/A| = 0.4$, $\phi_{D/C} = \pi/4$; and (f) $|B/A| = 0.4$, $\phi_{D/C} = \pi/2$.

single parameter $|B/A|$ in order to allow for a high fidelity as well as minimization of its sensitivity to $|\beta/\alpha|$, $\phi_{\beta/\alpha}$, and $\phi_{D/C}$. Since, as discussed in Sec. II C, $|B/A|$ is zero for electrons at the band edge and increases with the electron energy, the strategy for favorable fidelity characteristics would therefore be to move electron states to the band edge as close as possible.

V. CONCLUSION

In summary, we have investigated the valley-photon QST under a hybrid DBR and PC cavity setup that provides both an enhancement of the e-ph interaction and a spatial differentiation between incoming and outgoing photons at the same time. A quantum-mechanical analysis has been performed for the system consisting of electrons, trions, and photons, with the system being open to the environment and allowing for the photons to move in and out. Effects of damping are included. With the analysis, we have derived analytical expressions for the yield and fidelity, which suggest the following condition for an optimized yield: small trion damping rate, narrow photon band width, and nearly matching rates of photon emission by the trion into both cavities. It suggests the following condition for an optimized fidelity: placement of qubit electrons in near-band-edge states. Using realistic qubit and cavity parameters as well as optical matrix elements, a numerical study has also been carried out. A specific example is given with the following parameters: QD size ∼70 nm, photon frequency $\omega_{\rm ph} = 1.6 \cdot 10^5$ GHz corresponding to graphene band gap ∼0.1 eV, trion damping rate $\gamma_{SE} = 1$ GHz, photon band width $\Delta\omega_{\rm ph} = 5$ GHz, $Q \sim 550$ for the DBR cavity, and $Q \sim 250$ for the PC cavity. The calculation using the above parameters gives yield and fidelity both near unity.

In conclusion, results of this initial paper suggest that the unique valley-polarization correspondence in 2D hexagonal materials such as graphene can be exploited to enable valley-photon QST, with promising characteristics achievable under accessible conditions. Further experimental and theoretical explorations will be important to fully demonstrate such a quantum process as well as realize its full potential for 2D materials-based quantum technologies.

Last, we note that a similar idea of valley-photon QST may be applicable to TMDCs. However, owing to the existence of a strong spin-orbit interaction in TMDCs, spin and valley degrees of freedom are coupled, giving rise to a significant distinction between gapped graphene and TMDCs. An extensive work will therefore be required to generalize the valley-photon QST discussed here to TMDCs.

ACKNOWLEDGMENTS

We would like to thank MOST, ROC for supporting our paper through Contract No. 103-2119-M-007-007-MY3.

APPENDIX

Equation (17) can be solved by first considering the corresponding homogeneous equation, an eigenvalue problem for the matrix

$$H_0 = \begin{pmatrix} a & \sqrt{|A|^2+|B|^2} \\ \sqrt{|A|^2+|B|^2} & b \end{pmatrix}, \quad a \equiv \omega_{\text{trion}} - i\gamma_{\text{total}}, b \equiv \omega_{\text{PC}} - i\Gamma_{\text{PC}}. \tag{A1}$$

The solutions are given by the following eigenvalues

$$\lambda_1 = \frac{(a+b)+\sqrt{(a-b)^2+4(|A|^2+|B|^2)}}{2}, \quad \lambda_2 = \frac{(a+b)-\sqrt{(a-b)^2+4(|A|^2+|B|^2)}}{2}, \tag{A2}$$

and eigenvectors

$$|\varphi_1\rangle = \begin{pmatrix} \phi_{11} \\ \phi_{12} \end{pmatrix} = \begin{pmatrix} -\frac{-a+b+\sqrt{(a-b)^2+4(|A|^2+|B|^2)}}{2\sqrt{|A|^2+|B|^2}} \\ 1 \end{pmatrix}, \quad |\varphi_2\rangle = \begin{pmatrix} \phi_{21} \\ \phi_{22} \end{pmatrix} = \begin{pmatrix} -\frac{-a+b-\sqrt{(a-b)^2+4(|A|^2+|B|^2)}}{2\sqrt{|A|^2+|B|^2}} \\ 1 \end{pmatrix}. \tag{A3}$$

Next, we include the inhomogeneous part $f(t)$. We express $f(t)$ in terms of the eigenvectors of H_0:

$$f(t) = c_1(t)\begin{pmatrix} \phi_{11} \\ \phi_{12} \end{pmatrix} + c_2(t)\begin{pmatrix} \phi_{21} \\ \phi_{22} \end{pmatrix}, \tag{A4}$$

with the expansion coefficients given by

$$\begin{aligned} c_1(t) &= \frac{\phi_{22}}{\phi_{11}\phi_{22}-\phi_{12}\phi_{21}}\left[C\phi^{\text{DC}}_{\sigma_+K}(t) + D\phi^{\text{DC}}_{\sigma_-K}(t)\right] \\ c_2(t) &= \frac{-\phi_{12}}{\phi_{11}\phi_{22}-\phi_{12}\phi_{21}}\left[C\phi^{\text{DC}}_{\sigma_+K}(t) + D\phi^{\text{DC}}_{\sigma_-K}(t)\right] \end{aligned} \tag{A5}$$

It can be verified that the solution to Eq. (17) is given by

$$\begin{aligned} \begin{pmatrix} \phi^{\text{tri}}_K(t) \\ \phi^{\text{PC}}_{K1}(t) \end{pmatrix} = -i\Bigg[& \frac{\phi_{22}}{\phi_{11}\phi_{22}-\phi_{12}\phi_{21}}\begin{pmatrix} \phi_{11} \\ \phi_{12} \end{pmatrix}\int_0^t dt' e^{-i\lambda_1(t-t')} C\phi^{\text{DC}}_{\sigma_+K}(t') - \frac{\phi_{12}}{\phi_{11}\phi_{22}-\phi_{12}\phi_{21}}\begin{pmatrix} \phi_{21} \\ \phi_{22} \end{pmatrix}\int_0^t dt' e^{-i\lambda_2(t-t')} C\phi^{\text{DC}}_{\sigma_+K}(t') \\ & + \frac{\phi_{22}}{\phi_{11}\phi_{22}-\phi_{12}\phi_{21}}\begin{pmatrix} \phi_{11} \\ \phi_{12} \end{pmatrix}\int_0^t dt' e^{-i\lambda_1(t-t')} D\phi^{\text{DC}}_{\sigma_-K}(t') - \frac{\phi_{12}}{\phi_{11}\phi_{22}-\phi_{12}\phi_{21}}\begin{pmatrix} \phi_{21} \\ \phi_{22} \end{pmatrix}\int_0^t dt' e^{-i\lambda_2(t-t')} D\phi^{\text{DC}}_{\sigma_-K}(t')\Bigg] \end{aligned} \tag{A6}$$

Using Eq. (14) for the DBR cavity photon amplitude, it gives

$$\begin{aligned} \phi^{\text{PC}}_{K1}(t) = & -i\sqrt{c\kappa_{\text{DC}}}\phi^{\text{ph}}_0 \frac{\phi_{12}\phi_{22}}{\phi_{11}\phi_{22}-\phi_{12}\phi_{21}}[\alpha C + \beta D]\left[\int_0^t dt' e^{-i\lambda_1(t-t')} - \int_0^t dt' e^{-i\lambda_2(t-t')}\right] \\ & \times \int_{-\infty}^{\infty}\frac{d\omega}{2\pi} e^{\frac{-i(\omega-\omega_{\text{ph}})x_0}{c}} e^{\frac{-(\omega-\omega_{\text{ph}})^2}{2\Delta\omega^2_{\text{ph}}}} \frac{e^{i\omega t'} - e^{-i(\omega_{\text{DC}}-i\kappa_{\text{DC}}-iC)t'}}{(\omega+\omega_{\text{DC}}-i\kappa_{\text{total}})} \end{aligned} \tag{A7}$$

Now, substituting the above result into Eq. (24) and evaluating the resultant integral, we arrive at the final state amplitude when the QST is completed:

$$\begin{aligned} \lim_{x_0\to-\infty}\phi^{\text{output}}_{K1}(k_{2\text{D}},t\to\infty) = & -e^{-i\omega_{\text{output}}(k_{2\text{D}})t} T_k\sqrt{c\kappa_{\text{DC}}}\phi^{\text{ph}}_0 \frac{\phi_{12}\phi_{22}}{\phi_{11}\phi_{22}-\phi_{12}\phi_{21}}[\alpha C+\beta D] \\ & \times \frac{(\lambda_1-\lambda_2)}{(\omega_{\text{output}}(k_{2\text{D}})-\lambda_1)(\omega_{\text{output}}(k_{2\text{D}})-\lambda_2)(\omega_{\text{DC}}-i\kappa_{\text{total}}-\omega_{\text{output}}(k_{2\text{D}}))}. \end{aligned} \tag{A8}$$

This leads to the result in Eq. (25).

[1] A. Rycerz, J. Tworzydlo, and C.W. J. Beenakker, Nat. Phys. **3**, 172 (2007).

[2] D. Xiao, W. Yao, and Q. Niu, Phys. Rev. Lett. **99**, 236809 (2007).

[3] R. V. Gorbachev, J. C. W. Song, G. L. Yu, A. V. Kretinin, F. Withers, Y. Cao, A. Mishchenko, I. V. Grigorieva, K. S. Novoselov, L. S. Levitov, and A. K. Geim, Science **346**, 448 (2014).

[4] H. Zeng, J. Dai, W. Yao, and X. Cui, Nat. Nanotechnol. **7**, 490 (2012).

[5] K. F. Mak, K. He, J. Shan, and T. F. Heinz, Nat. Nanotechnol. **7**, 494 (2012).

[6] Q. H. Wang, K. Kalantar-Zadeh, A. Kis, J. N. Coleman, and M. S. Strano, Nat. Nanotechnol. **7**, 699 (2012).

[7] Y. J. Zhang, T. Oka, R. Suzuki, J. T. Ye, and Y. Iwasa, Science **344**, 725 (2014).

[8] W. Yao, D. Xiao, and Q. Niu, Phys. Rev. B **77**, 235406 (2008).

[9] K. S. Novoselov, A. K. Geim, S. V. Morozov, D. Jiang, Y. Zhang, S. V. Dubonos, I. V. Grigorieva, and A. A. Firsov, Science **306**, 666 (2004); A. K. Geim and K. S. Novoselov, Nat. Mater. **6**, 183 (2007).

[10] Y. Zhang, Y.-W. Tan, H. L. Stormer, and P. Kim, Nature **438**, 201 (2005).

[11] A. H. Castro Neto, F. Guinea, N. M. R. Peres, K. S. Novoselov, and A. K. Geim, Rev. Mod. Phys. **81**, 109 (2009).

[12] K. F. Mak, C. Lee, J. Hone, J. Shan, and T. F. Heinz, Phys. Rev. Lett. **105**, 136805 (2010).

[13] G. Y. Wu, N.-Y. Lue, and L. Chang, Phys. Rev. B **84**, 195463 (2011).

[14] N. Rohling and G. Burkard, New J. Phys. **14**, 083008 (2012); N. Rohling, M. Russ, and G. Burkard, Phys. Rev. Lett. **113**, 176801 (2014).

[15] G. Y. Wu, N.-Y. Lue, and Y.-C. Chen, Phys. Rev. B **88**, 125422 (2013).

[16] A. Kormányos, V. Zólyomi, N. D. Drummond, and G. Burkard, Phys. Rev. X **4**, 011034 (2014).

[17] Y. Wu, Q. Tong, G.-B. Liu, H. Yu, and W. Yao, Phys. Rev. B **93**, 045313 (2016).

[18] M. T. Allen, J. Martin, and A. Yacoby, Nature Commun. **3**, 934 (2012).

[19] X.-X. Song, D. Liu, V. Mosallanejad, J. You, T.-Y. Han, D.-T. Chen, H.-O. Li, G. Cao, M. Xiao, G.-C. Guo, and G.-P. Guo, Nanoscale. **7**, 16867 (2015)

[20] K. Wang, T. Taniguchi, K. Watanabe, and P. Kim, arXiv:1610.02929 (2016).

[21] C. G. Yale, F. J. Heremans, B. B. Zhou, A. Auer, G. Burkard, and D. D. Awschalom, Nature Photonics **10**, 184 (2016) and references therein.

[22] F. Xia, H. Wang, D. Xiao, M. Dubey, and A. Ramasubramaniam, Nature Photon. **8**, 899 (2014).

[23] X. Liu and V. M. Menon, IEEE J. Quantum Electron. **51**, (2015).

[24] X. Liu, T. Galfsky, Z. Sun, F. Xia, E. C. Lin, Y. H. Lee, S. Kena-Cohen, and V. M. Menon, Nature Photon. **9**, 30 (2015).

[25] X. Gan, Y. Gao, K. F. Mak, X. Yao, R.-J. Shiue, A. van der Zande, M. E. Trusheim, F. Hatami, T. F. Heinz, J. Hone, and D. Englund, Appl. Phys. Lett. **103**, 181119 (2013).

[26] G. Y. Wu and N.-Y. Lue, Phys. Rev. B **86**, 045456 (2012).

[27] Y. Rikitake, H. Imamura, and H. Kosaka, J. Phys. Soc. Jpn. **76**, 114004 (2007).

[28] D. A. Lidar, I. L. Chuang, and K. B. Whaley, Phys. Rev. Lett. **81**, 2594 (1998); M. Mohseni and D. A. Lidar, *ibid.* **94**, 040507 (2005).

[29] J. I. Cirac, P. Zoller, H. J. Kimble, and H. Mabuchi, Phys. Rev. Lett. **78**, 3221 (1997); H. J. Briegel, W. Dur, J. I. Cirac, and P. Zoller, *ibid.* **81**, 5932 (1998); L.-M. Duan, M. D. Lukin, J. J. Cirac, and P. Zoller, Nature **414**, 413 (2001).

[30] H. J. Kimble, Nature **453**, 1023 (2008).

[31] B. B. Blinov, D. L. Moehring, L.-M. Duan, and C. Monroe, Nature **428**, 153 (2004).

[32] T. Chanelière, D. N. Matsukevich, S. D. Jenkins, S.-Y. Lan, T. A. B. Kennedy, and A. Kuzmich, Nature **438**, 833 (2005).

[33] A. Stute, B. Brandstatter, K. Friebe, T. E. Northup, and R. Blatt, Nature Photon. **7**, 219 (2013).

[34] C. Kurz, M. Schug, P. Eich, J. Huwer, P. Műller, and J. Eschner, Nature Commun. **5**, 5527 (2014).

[35] M. A. Sillanpää, J. I. Park, and R. W. Simmonds, Nature **449**, 438 (2007); M. Hua, M.-J. Tao and F.-G. Deng, Scientific Reports **6**, 22037 (2016); P. Xu, X.-C. Yang, F. Mei, and Z.-Y. Xue, *ibid.* **6**, 18695 (2016).

[36] E. Togan, Y. Chu, A. S. Trifonov, L. Jiang, J. Maze, L. Childress, M. V. G. Dutt, A. S. Sørensen, P. R. Hemmer, A. S. Zibrov, and M. D. Lukin, Nature **466**, 730 (2010).

[37] N. Y. Yao, L. Jiang, A. V. Gorshkov, Z.-X. Gong, A. Zhai, L.-M. Duan, and M. D. Lukin, Phys. Rev. Lett. **106**, 040505 (2011).

[38] H. Kosaka, H. Shigyou, Y. Mitsumori, Y. Rikitake, H. Imamura, T. Kutsuwa, K. Arai, and K. Edamatsu, Phys. Rev. Lett. **100**, 096602 (2008).

[39] H. Kosaka, T. Inagaki, Y. Rikitake, H. Imamura, Y. Mitsumori, and K. Edamatsu, Nature **457**, 702 (2009).

[40] M. A. Nielsen and I. L. Chuang, *Quantum Computation and Quantum Information* (Cambridge University Press, Cambridge, 2003) and references therein.

[41] A. Kitaev, Ann. Phys. **303**, 2 (2003); C. Nayak, S. H. Simon, A. Stern, M. Freedman, and S. D. Sarma, Rev. Mod. Phys. **80**, 1083 (2008).

[42] H. Ryu, S. Kim, H. Park, J. Hwang, Y. Lee, and J. Kim, Appl. Phys. Lett. **80**, 3883 (2002).

[43] Y. Akahane, T. Asano, B. Song, and S. Noda, Nature **425**, 944 (2003).

[44] Y. Wakayama, A. Tandaechanurat, S. Iwamoto, and Y. Arakawa, Opt. Express **16**, 21321 (2008).

[45] R. Nascimento, J. da Rocha Martins, R. J. C. Batista, and H. Chacham, J. Phys. Chem. C **119**, 5055 (2015).

[46] H.-C. Cheng, N.-Y. Lue, Y.-C. Chen, and G. Y. Wu, Phys. Rev. B **89**, 235426 (2014).

[47] O. Painter and K. Srinivasan, Phys. Rev. B **68**, 035110 (2003).